AIMS Biophysics

AIMS Biophysics, 10(3): 401–439.
DOI: 10.3934/biophy.2023024
Received: 14 April 2023
Revised: 26 August 2023
Accepted: 12 September 2023
Published: 26 September 2023

http://www.aimspress.com/journal/biophysics

*Research article*

# Quantum mechanical aspects of cardiac arrhythmias: A mathematical model and pathophysiological implications

**Mohammed I. A. Ismail[1], Abdallah Barjas Qaswal[2,*], Mo'ath Bani Ali[3], Anas Hamdan[4], Ahmad Alghrabli[5], Mohamad Harb[5], Dina Ibrahim[5], Mohammad Nayel Al-Jbour[6], Ibrahim Almobaiden[7], Khadija Alrowwad[8], Esra'a Jaibat[9], Mira Alrousan[9], Mohammad Banifawaz[10], Mohammed A. M. Aldrini[10], Aya Daikh[11] , Nour Aldarawish[12], Ahmad Alabedallat[4], Ismail M. I. Ismail[13] and Lou'i Al-Husinat[14]**

[1] Anesthesiology Department, Mut'ah School of Medicine, Al-Karak 61710, Jordan
[2] Department of Psychiatry, Jordan University Hospital, Amman 11942, Jordan
[3] Department of Internal Medicine, King Hussein Center, Amman 11942, Jordan
[4] Department of Anesthesia and Intensive Care Unit, Istishari Hospital, Amman 11184, Jordan
[5] Department of Internal Medicine, Jordan University Hospital, Amman 11942, Jordan
[6] King Hussein Medical Center, King Abdullah II St 230, Amman 11185, Jordan
[7] Department of Emergency Medicine, Jordan University Hospital, Amman 11942, Jordan
[8] Department of Pediatrics, Jordan University Hospital, Amman 11942, Jordan
[9] Department of Family Medicine, Jordan University Hospital, Amman 11942, Jordan
[10] Department of General Surgery, Jordan University Hospital, Amman 11942, Jordan
[11] Medical Doctor at Hospital D'aoulef, Aoulef, Algeria
[12] School of Medicine, Mutah University, Al-Karak 61710, Jordan
[13] Medical student, Jordan University of Science and Technology, Irbid, Jordan
[14] Department of Clinical Medical Sciences, Faculty of Medicine, Yarmook University, Irbid 21163, Jordan

* **Correspondence:** Email: qaswalabdullah@gmail.com.

**Abstract:** Cardiac arrhythmias are serious myocardial electrical disturbances that affect the rate and rhythm of heartbeats. Despite the rapidly accumulating data about the pathophysiology and the treatment, new insights are required to improve the overall clinical outcome of patients with cardiac arrhythmias. Three major arrhythmogenic processes can contribute to the pathogenesis of cardiac arrhythmias; 1) enhanced automaticity, 2) afterdepolarization-triggered activity and 3) reentry circuits.

The mathematical model of the quantum tunneling of ions is used to investigate these mechanisms from a quantum mechanical perspective. The mathematical model focuses on applying the principle of quantum tunneling to sodium and potassium ions. This implies that these ions have a non-zero probability of passing through the gate, which has an energy that is higher than the kinetic energy of ions. Our mathematical findings indicate that, under pathological conditions, which affect ion channels, the quantum tunneling of sodium and potassium ions is augmented. This augmentation creates a state of hyperexcitability that can explain the enhanced automaticity, after depolarizations that are associated with triggered activity and a reentry circuit. Our mathematical findings stipulate that the augmented and thermally assisted quantum tunneling of sodium and potassium ions can depolarize the membrane potential and trigger spontaneous action potentials, which may explain the automaticity and afterdepolarization. Furthermore, the quantum tunneling of potassium ions during an action potential can provide a new insight regarding the formation of a reentry circuit. Introducing these quantum mechanical aspects may improve our understanding of the pathophysiological mechanisms of cardiac arrhythmias and, thus, contribute to finding more effective anti-arrhythmic drugs.

**Keywords:** quantum tunneling; ions; voltage-gated channel; arrhythmia; quantum biology

## 1. Introduction

Cardiac arrhythmias represent a major health issue that affects the normal electrophysiology of cardiac cells and leads to sudden cardiac death [1–3]. Several pathological causes and risk factors are implicated in the development of various electrical abnormalities in the heart, including ischemic heart disease, cardiomyopathy, inherited channelopathies, myocarditis, electrolyte disturbances and drug-induced disturbances [4–9]. These cardiac arrhythmias include atrial flutter, atrial fibrillation, paroxysmal supraventricular tachycardia, ventricular tachycardia and ventricular fibrillation, which all frequently occur in critical care unit patients. Three major pathophysiological processes are involved in the pathogenesis of cardiac arrhythmias. These include increased automaticity, triggered activity due to afterdepolarization and the formation of a reentry circuit [10,11]. Enhanced automaticity abnormally develops in the atrial and ventricular cardiac cells when a depolarization of the membrane potential occurs, in the range of −70 mV to −30 mV above the normal potential of −90 mV of cardiac cells [10,11]. In this case, the ventricles and atria are now capable of inducing spontaneous action potentials, and, as the membrane potential becomes depolarized, the rate of spontaneous activity increases [10,11]. Triggered activity is associated with afterdepolarizations, which are classified as early afterdepolarization (EAD) or late afterdepolarization (DAD) [10,11]. EADs develop during the phase of the repolarization of an action potential, while DADs develop after the full repolarization phase has occurred [10,11]. EADs occur when the inward cationic current predominates over the outward cationic current, and this includes a decrease in the potassium current and an increase in the sodium and calcium currents [10,11]. The reentry circuit is formed when two adjacent fibers, which are connected anatomically proximally and distally, have different values of conduction velocity and refractory periods [10,11]. When a fiber with slow conduction and a short refractory period initiates an impulse at the proximal connection, the impulse will be conducted back to the original site via the other fiber that has fast conduction and a long refractory period [10,11]. This will form a pathological reentry circuit that results in cardiac tachyarrhythmia [10,11]. The reentry circuit will form two types

of conduction i.e., anterograde and retrograde conduction, which contribute to the persistence of tachyarrhythmia. All of these pathological mechanisms occur much more frequently in the presence of hypoxia, acidosis, ischemia, infarction, channelopathies, inflammation and/or mechanical stretch, which are commonly found in critical care unit patients [4–9,12–15]. All of these risk factors can decrease the energy barrier of the closed gate of voltage-gated channels, and this can facilitate the passage of ions [16–18]. The decrease in the energy barrier is represented by a decrease in the half-activation voltage, which results in a left-shift in the activation curve, and an increase in the half-inactivation voltage, which results in a right-shift in the inactivation curve [16–18].

Despite the advances in cardiac electrophysiology and cardiac pharmacology, there is no universal consensus on the pathophysiological mechanisms behind cardiac arrhythmias, nor a definitive and obvious cure for them. Furthermore, the classical antiarrhythmic drugs can cause arrhythmias, which is a paradoxical undesirable effect [19–22]. All of these problematic issues represent a reasonable motivation to revisit our classical understanding of the basic mechanisms of cardiac arrhythmias. The fields of cardiology and electrophysiology are mostly based on classical physics. Hence, in the present paper, we plan to conceptualize the three major mechanisms of cardiac arrhythmias by using the principles of quantum mechanics that are applied to ions within their channels. This may help to fill the gaps in our comprehension of how these arrhythmias develop and, hopefully, to find more efficacious antiarrhythmic pharmacological agents that do not cause any paradoxical arrhythmic effect and decrease the overall mortality among patients who receive these medications.

Exploring the cellular and biological processes from the quantum mechanical perspective has garnered more attention in recent years [23–25]. This approach falls under the umbrella of quantum biology, or even quantum medicine. Quantum biology is the scientific field that addresses the intersection between biology and quantum mechanics. It focuses on describing the behavior of particles, including electrons, protons, ions and molecules, by using the principles of quantum mechanics, which include quantum coherence, quantum tunneling, quantum entanglement and quantum spin interactions. This quantum behavior can be used to explain certain biological processes and actions [23–25]. This approach is purposed to complement the classical approach and provide a comprehensive understanding of the physiological and pathological processes occurring in the biological environment [23–25]. Examples of such processes include proton tunneling in DNA mutations and enzymes [26,27]. Thus, our study adopts such an approach to augment our knowledge regarding cardiac arrhythmias and their pathogenesis. In the present paper, we will show how the quantum approach can explain the three pathological mechanisms, as well as show its distinctive features that make it unique from the classical approach. To this end, a model of the quantum tunneling of ions through the gates of channels [28] has been utilized. Quantum tunneling is a quantum phenomenon in which a particle has a non-zero probability of passing through a barrier that has an energy that is higher than the energy of the particle [29]. Hence, when this idea is applied to ions, they can be viewed as a quantum particle whose wavefunction can tunnel through a closed gate that is classically impenetrable [29]. This model will help us to explore the quantum transport of ions and its association with the pathogenesis of cardiac arrhythmias.

## 2. Mathematical model of the quantum tunneling of ions through the closed gate of voltage-gated channels

### *2.1. The ion quantum tunneling probability and the quantum conductance*

The quantum tunneling model in the present study is applied to the voltage-gated channels, particularly, the closed gate. The closed gate seals off the permeation of ions by forming an energy barrier that blocks their passage [30–32]. Previous studies have determined the shapes of the barrier by using the potential mean forces (PMFs) of the closed gate while experimentally focusing on the hydrophobic gating mechanism in which dewetting increases the barrier energy and wetting decreases it [30,33,34]. (De)wetting is the process of (de)hydration, which is related to the strength of the hydrophobic interactions and, thus, with the value of the energy barrier of the closed gate. The higher the hydration in the pore, the lower the energy barrier that can block the permeation of ions, and vice versa. The shape of the barrier obtained in the previous studies can be approximated by using the symmetric Eckart potential barrier [35,36].

The Wentzel–Kramers–Brillouin approximation of the one-dimensional quantum tunneling probability of a particle hitting a potential barrier can be mathematically represented by the following equation [29,37]:

$$T_Q = e^{\frac{-\sqrt{8m}}{\hbar}\int_{x_1}^{x_2}\sqrt{U(x)-KE}\,dx}, \tag{1}$$

where $T_Q$ is the tunneling probability of ions, $\hbar$ is the reduced Planck's constant ($1.05\times10^{-34}$ Js), $m$ is the mass of an ion ($m_{Na}=3.8\times10^{-26}$ Kg and $m_K=6.5\times10^{-26}$ Kg), $x$ is the ion's position in the gate, $U(x)$ is the function of the barrier's potential energy and $KE$ is the kinetic energy of the ion.

In the present study, we adopt two possible shapes for the potential energy profile of the closed gate based on the previous studies. These shapes are the aforementioned symmetric Eckart barrier and the rectangular barrier. See Figure 1. Choosing another barrier shape, which is the rectangular barrier, enables comparison and the ability to assess the influence of changing the shape of the barrier on the quantum tunneling process and, thus, on the overall pathogenesis of cardiac arrhythmias. The symmetric Eckart potential can be mathematically represented by the following equation [35,36,38]:

$$U(x)=\frac{G}{\cosh^2(\frac{x}{L})}, \tag{2}$$

where $G$ is the barrier height of the closed gate and $L$ is the length of the gate at which $U(\mathrm{L})=0.42\,\mathrm{G}$.

On the other hand, the potential of the rectangular barrier can be mathematically represented by the following equation [35,36]:

$$U(x)=G, \tag{3}$$

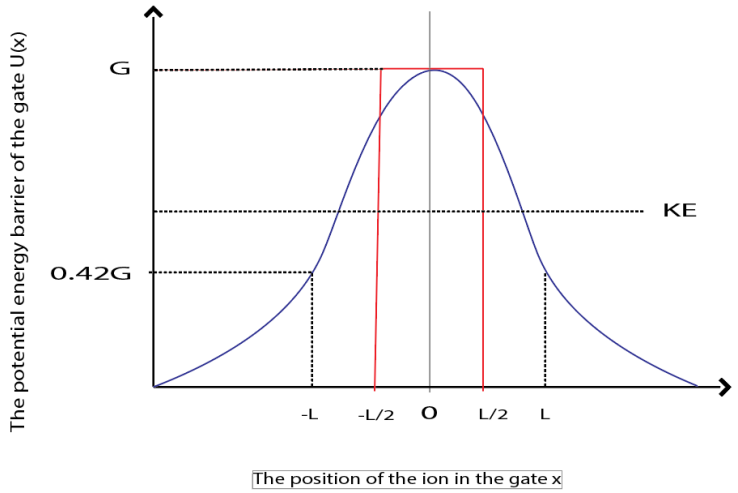


**Figure 1.** A schematic diagram of two possible energy barriers of the closed gate. The symmetric Eckart barrier (shown in blue) and the rectangular barrier (shown in red).

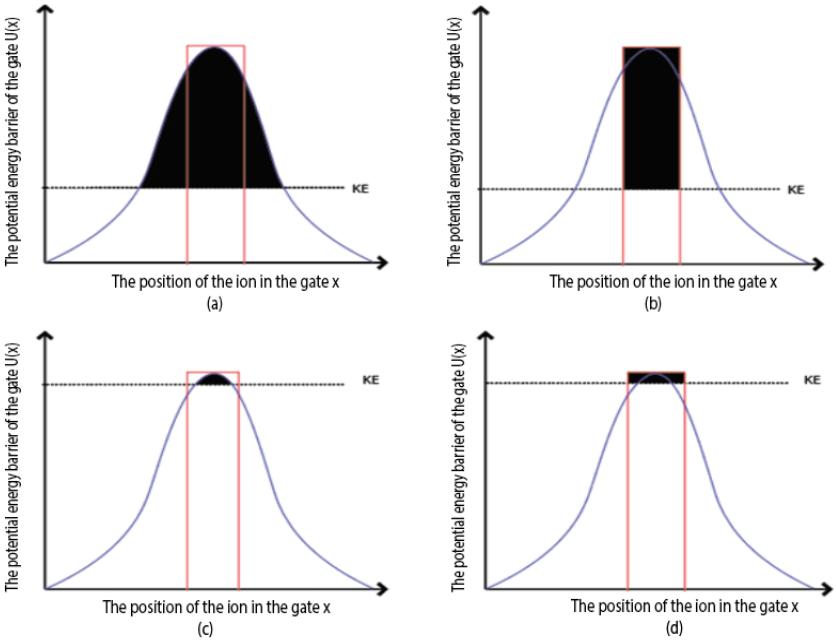


**Figure 2.** A schematic diagram that illustrates the effect of the kinetic energy of the ion on the area under the curve, which is inversely proportional to the tunneling probability, as indicated in Equation (1). It is clear that, as the level of the kinetic energy increases, the surface area between the curve and the constant line of kinetic energy decreases; thus, the tunneling probability increases. If the line of the kinetic energy is below the level of the intersection between the Eckart barrier and the rectangular barrier, then the rectangular barrier will have less surface area and, thus, higher tunneling probability, as represented in (a) and (b), and vice versa in (c) and (d).

By a close observation of Equation (1), we can see that the integral part is proportional to the surface area enclosed between the function *U(x)* and the constant line of kinetic energy *KE*. See

Figure 2. This means that a larger surface area indicates lower tunneling probability, and vice versa. This concept will be useful in facilitating a comparison between the two barriers and predicting the differences between them according to the values of barrier height *G* and the kinetic energy *KE*.

According to Figure 2, when the constant line of kinetic energy is far below the intersection of the two barriers, as in Figure 2a and 2b, the area under the curve for the rectangular barrier is less than that for the Eckart barrier. Hence, it is expected that the tunneling probability will be higher for the rectangular barrier. On the other hand, when the line of kinetic energy is above the intersection, the area under the curve for the Eckart barrier is less than that for the rectangular barrier, as in Figure 2c and 2d, hence, the tunneling probability will be higher for the Eckart barrier.

If the tunneling probability of a particle through the Eckart potential is considered, the tunneling probability can be calculated by using the following equation [35,38]:

$$T_Q = \frac{cosh\left(2\pi\left(2\alpha\right)\right) - 1}{cosh\left(2\pi\left(2\alpha\right)\right) + cosh\left(2\pi\delta\right)}, \tag{4}$$

where $\alpha = \frac{L}{2\hbar}\sqrt{2mKE}$, $\delta = \frac{1}{2}\sqrt{(\frac{16\pi^2L^2}{h^2})2\,\mathrm{Gm} - 1}$ (the −1 under the square root will be neglected in the following calculations because it does not significantly affect the results), *L* is the length of the gate (at which U(L) = 0.42 G), *m* is the mass of the ion, *KE* is the kinetic energy of the ion, *G* is the barrier height of the gate, *h* is the Planck constant ($6.6\times10^{-34}$ Js) and $\hbar$ is the reduced Planck constant ($1.05\times10^{-34}$ Js). To reduce the complexity of the mathematics in Equation (4) while maintaining the consistency and reasonability of the numerical results, the following approximation can be used [35,38]: $cosh\, x \approx \frac{1}{2}e^x$ for any $x \geq 3$. This can be easily checked by substituting the following values: $L = 1\times10^{-10}$ m, $m_{Na} = 3.8\times10^{-26}$ kg, $KE = 1\times10^{-20}$ J and $G = 1\times10^{-20}$ J in α and δ. These values will become reasonable in the following sections. Consequently, Equation (4) can be rewritten as follows [35,38]:

$$T_Q \approx \frac{e^{2\pi.2\alpha}}{e^{2\pi.2\alpha} + e^{2\pi\delta}} \approx \frac{1}{\frac{e^{2\pi.2\alpha} + e^{2\pi\delta}}{e^{2\pi.2\alpha}}} \approx \frac{1}{1 + e^{2\pi(\delta - 2\alpha)}} \approx e^{-2\pi(\delta - 2\alpha)}. \tag{5}$$

The "−1" in the numerator of Equation (4) and the "1" in the denominator in Equation (5) can be neglected.

Eventually, by substituting the values of $\alpha$ and $\delta$ in Equation (5), the quantum tunneling of ions through the Eckart potential can be calculated by using the following equation [35,38]:

$$T_{Q-Eckart} = e^{-\lambda L(\sqrt{G} - \sqrt{KE})}, \tag{6}$$

where $\lambda = \frac{\sqrt{8\pi^2 m}}{\hbar}$ and *L* is the length of the gate at which $U(L) = 0.42G$.

The equation to describe the tunneling through the rectangular barrier can be obtained by substituting the energy profile $U(x) = G$ in Equation (1) and solving the integral as follows: [36,37]:

$$T_Q = e^{\frac{-\sqrt{8m}}{\hbar}\int_{x_1}^{x_2}\sqrt{G-KE}dx} = e^{\frac{-\sqrt{8m}}{\hbar}\sqrt{G-KE}(x_2-x_1)} = e^{\frac{-\sqrt{8m}}{\hbar}L\sqrt{G-KE}}. \quad (7)$$

Accordingly, the quantum tunneling of ions through the rectangular barrier can be calculated by using the following equation:

$$T_{Q-\text{Rectangular}} = e^{-\omega L\sqrt{G-KE}}, \quad (8)$$

where $\omega = \frac{\sqrt{8m}}{\hbar}$ and $L$ is the length of the gate, which is the width of the rectangular barrier.

Equation (6) and Equation (8) will be considered in further investigation to compare between these barrier shapes. When some studies examined the hydrophobic gating experimentally [39–41], the barrier shapes could not be represented by a concrete mathematical function due to the irregularities and asymmetries that deviate from the symmetric Eckart potential. However, if it is compared with the shapes used in this study in terms of the area under the curve, it becomes more feasible to estimate how such shapes can affect the quantum tunneling of ions based on the idea of the area under the curve. See Figure 3.

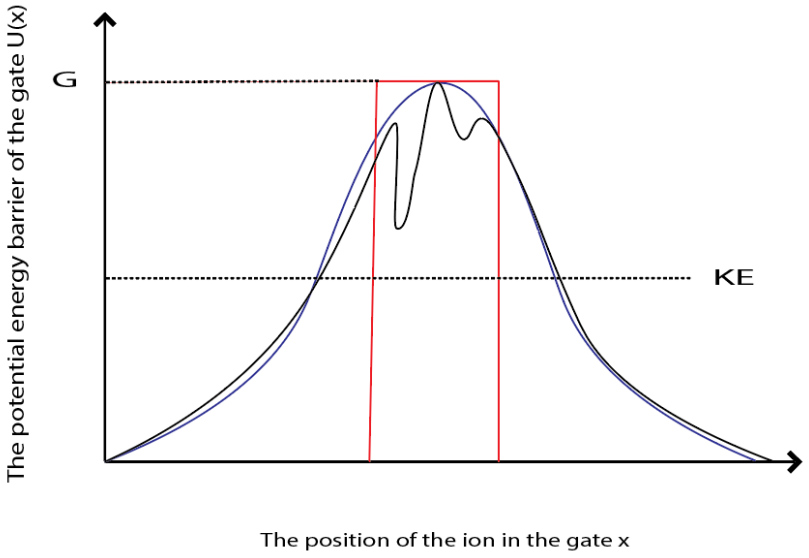


**Figure 3.** A schematic diagram of three possible shapes of the potential energy profile of the closed gate. These shapes are the symmetric Eckart barrier (in blue), the rectangular barrier (in red) and the asymmetric shape (in black) that may be obtained experimentally.

Using the idea of area under the curve and applying it to the contents of Figure 3, one can estimate that the area under the curve of the asymmetric shape is less than that for the Eckart barrier, but larger than that for the rectangular. Thus, the tunneling probability for the asymmetric barrier is higher than that for the Eckart barrier, but less than that for the rectangular barrier. The presence of such dips in the asymmetric shape is due to the drops in the energy barrier that result from hydration or wetting [39–41]. The symmetry of the barrier shape is determined by the orientation and the arrangement of the

hydrophobic substances or materials. As the hydrophobic composition of the barrier is homogeneous with minimal or no hydrophilic composition, the shape of the barrier will be more symmetrical with minimal hydration and, thus, minimal deviations from symmetry [42–45]. Therefore, choosing the shape of the barrier depends on the hydrophobic homogeneity of the physical barrier, which can be manipulated experimentally to show the influence of the shape on the quantum tunneling of ions, as we are going to explain in the next sections. Hence, this can be an experimental approach to provide evidence of the existence of the quantum behavior of ions.

The quantum unitary conductance of ion channels can be calculated by using the following equation [35–37,46]:

$$C_Q = \frac{q^2}{h} T_Q , \tag{9}$$

where $q$ is the charge of the ion ( $1.6\times10^{-19}$ C), $h$ is the Planck constant ( $6.6\times10^{-34}$ Js) and $T_Q$ is the quantum tunneling probability.

The quantum membrane conductance $MC_Q$ can be calculated by using the following equation [47]:

$$MC_Q = C_Q \times D, \tag{10}$$

where $D$ is the number of ion channels per surface area unit or the density of ion channels (channels/cm$^2$).

The quantum conductance is crucial in the assessment of the influence of the quantum tunneling of sodium and potassium ions on the membrane potential, excitability and the pathogenesis of cardiac arrhythmias.

The closed gate is located at the intracellular end of the cellular membrane and it is sealed off by four hydrophobic residues from the four S6 alpha helices [30–32]. Therefore, the extracellular cations go through the membrane potential $V_m$, acquiring a kinetic energy of $qV_m$ until hitting the intracellular gate. On the other hand, the intracellular cations hit the closed gate before going through the membrane. See Figure 4.

Accordingly, the kinetic energy of the extracellular and intracellular cations can be calculated by using the following equations, respectively:

$$KE_o = qV_m + \frac{1}{2} K_B T , \tag{11}$$

$$KE_i = \frac{1}{2} K_B T . \tag{12}$$

Thus, it is clear that extracellular ions have higher kinetic energy and, thus, higher tunneling probability. See Figure 4.

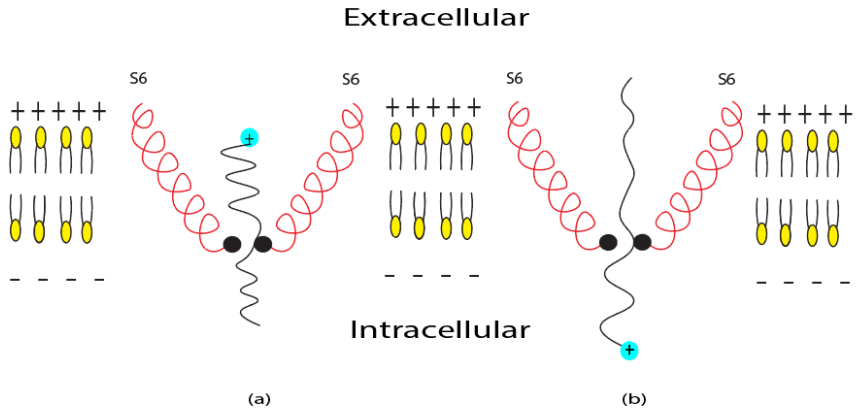


**Figure 4.** A schematic diagram of the voltage-gated channel. Two of the four alpha S6 helices are shown for simplicity. The intracellular gate is represented by two hydrophobic residues (shown by black dots) sealing off the permeation of ions. (a): The extracellular ion has higher kinetic energy, which is represented by the higher frequency of quantum waves, and thus higher tunneling probability, which is represented by a higher wave amplitude after tunneling through the gate. (b): The intracellular ion has lower kinetic energy, which is represented by the lower frequency of quantum waves, and thus lower tunneling probability, which is represented by lower wave amplitude after tunneling through the gate.

### 2.2. *The quantum tunneling-induced membrane depolarization*

In the present study, we will rely on the quantum version of the Goldman-Hodgkin-Katz (GHK) equation to evaluate the effect of quantum tunneling on the membrane potential [47].

The quantum version of the GHK equation is mathematically represented by the following expression [47]:

$$MC_{Na}[Na]_o + MC_K[K]_o + MC_{Qion-o}[ion]_o = e^{-\frac{qV_m}{K_BT}}(MC_{Na}[Na]_i + MC_K[K]_i + MC_{Qion-i}[ion]_i), \quad (13)$$

where the parameter definitions are as follows:

$MC_{Qion-o}$ is the quantum membrane conductance of an extracellular ion, $MC_{Qion-i}$ is the quantum membrane conductance of an intracellular ion, $[ion]_o$ is the extracellular concentration of the ion, $[ion]_i$ is the intracellular concentration of the ion, $MC_{Na}$ is the classical leaky membrane conductance of sodium ions ($0.005\,\text{mS/cm}^2$), $MC_K$ is the classical leaky membrane conductance of potassium ions ($0.5\,\text{mS/cm}^2$), $[Na]_o$ is the extracellular concentration of sodium ions (142 mmol/L), $[K]_o$ is the extracellular concentration of potassium ions (4 mmol/L), $[Na]_i$ is the intracellular concentration of sodium ions (14 mmol/L), $[K]_i$ is the intracellular concentration of potassium ions (140 mmol/L), $K_B$ is the Boltzmann constant ($1.38\times10^{-23}$ J/K), $T$ is the absolute temperature of human body (310 K), $q$ is the charge of the ion and $V_m$ is the membrane potential.

Based on aforementioned values of concentration and conductance, the resting membrane potential is 0.087 V without considering the quantum conductance or under the condition that the quantum tunneling is too weak to affect the membrane potential. This initial value of membrane potential will be used for cardiac cells to perform further analysis in the next sections.

### *2.3. The thermally assisted quantum tunneling-induced membrane depolarization*

The thermal energy within the biological environment can aid in augmenting the quantum tunneling probability by providing extra energy to decrease the energy barrier of the gate. See Figure 5.

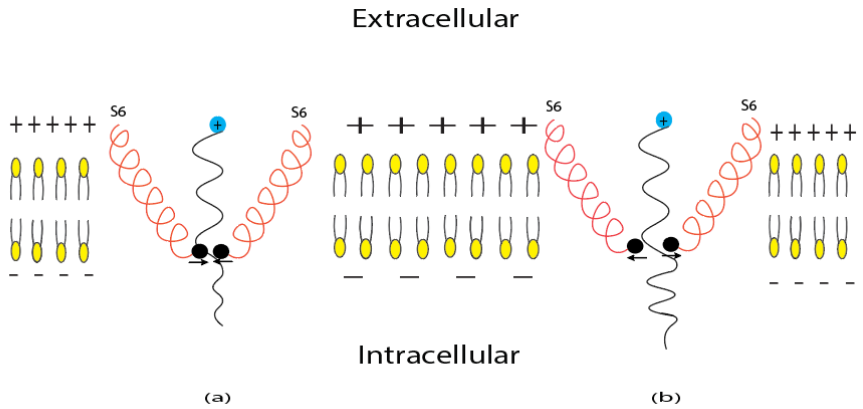


**Figure 5.** A schematic diagram that shows the process through which the thermal energy can contribute to enhancing the quantum tunneling probability of ions by lowering the energy barrier of the gate. (a): A cation projects toward a closed gate with a higher barrier height (*G)*, as indicated by the shorter distance between the residues. This results in the lower tunneling probability being represented by the lower wave amplitude after passing through the gate. (b): A cation projects toward a closed gate with a lower barrier height (*G)*, as indicated by the longer distance between the residues mediated by the thermal energy. This results in a higher tunneling probability being represented by the higher wave amplitude after passing through the gate.

The mathematical representation of the thermally augmented tunneling probability can be given by the following equation:

$$T_{Q-thermal} = \sum_{0}^{E \le G-KE} \frac{1}{\beta} e^{\frac{-E}{\beta}} e^{\frac{-\sqrt{8m}}{\hbar}\int_{x_1}^{x_2}\sqrt{U(x)-\mathrm{E}-KE}dx} \quad . \tag{14}$$

Equation (14) calculates the average quantum tunneling probability when the thermal energy $E$ is exploited to decrease the energy barrier of the gate. This is achieved by finding the sum of multiplying the probability of finding the thermal energy $E$ with the corresponding tunneling probability. However, since the values of $E$ are continuous and not discrete, we use the integral form as in the following equation:

$$T_{Q-thermal} = \frac{1}{\beta}\int_{0}^{E\le G-KE} e^{\frac{-E}{\beta}} e^{\frac{-\sqrt{8m}}{\hbar}\int_{x_1}^{x_2}\sqrt{U(x)-E-KE}dx} dE, \quad (15)$$

where $\beta = K_B T$ and $E$ is the tunneling-assistive thermal energy. Hence, the thermally assisted quantum membrane conductance can be calculated by using the following equation:

$$MC_{Q-thermal} = \sigma\int_{0}^{E\le G-KE} e^{\frac{-E}{\beta}} e^{\frac{-\sqrt{8m}}{\hbar}\int_{x_1}^{x_2}\sqrt{U(x)-E-KE}dx} dE, \quad (16)$$

where $\sigma = \frac{Dq^2}{h\beta}$, which is derived based on Equation (9) and Equation (10).

Therefore, the thermally assisted quantum membrane conductance for the Eckart barrier and the rectangular barrier can be calculated by using the following equations, respectively:

$$MC_{Q-thermal(Eckart)} = \sigma\int_{0}^{E\le G-KE} e^{\frac{-E}{\beta}} e^{-\lambda L(\sqrt{G}-\sqrt{KE})} dE, \quad (17)$$

$$MC_{Q-thermal(\text{rectangular})} = \sigma\int_{0}^{E\le G-KE} e^{\frac{-E}{\beta}} e^{-\omega L\sqrt{G-KE}} dE. \quad (18)$$

Integrating Equations (17) and (18) and incorporating the results into the GHK equation, the thermally assisted quantum version of the GHK equation can be represented by the following equation:

$$MC_{Na}[Na]_o + MC_K[K]_o + MC_{Q-thermal(o)}[ion]_o = e^{-\frac{qV_m}{K_B T}}(MC_{Na}[Na]_i + MC_K[K]_i + MC_{Q-thermal(i)}[ion]_i), \quad (19)$$

### *2.4. The classical opening of voltage-gated channels*

Classically, voltage-gated channels operate by dilating the narrowed pore of the closed gate. This dilation will separate the hydrophobic residues, and the radius of the pore increases. This will increase the probability of hydration, thus lowering the barrier height of the gate so that the ions are now more likely to have an energy that is equivalent to or higher than the barrier height [30,33,34].

The membrane conductance due to the classical opening of voltage-gated channels can be calculated by using the following equation:

$$MC_{classical} = P_{open} C_{open} D, \quad (20)$$

where $P_{open} = \frac{1}{1+e^{\frac{G}{\beta}}}$ is the probability of opening closed channels, $C_{open}$ is the conductance of open channels and $D$ is the number of channels per surface area unit.

Thus, we can use the GHK equation to assess the influence of the classical opening of voltage-gated channels on the membrane potential:

$$MC_{Na}[Na]_o + MC_K[K]_o + [ion]_o \frac{DC_{open(mS)}}{1+e^{\frac{G}{\beta}}} = e^{-\frac{qV_m}{K_B T}} (MC_{Na}[Na]_i + MC_K[K]_i + [ion]_i \frac{DC_{open(mS)}}{1+e^{\frac{G}{\beta}}}), \quad (21)$$

where $C_{open(mS)}$ is the conductance of the voltage-gated channel when the gate is classically open. The unit will be mS, so the membrane conductance will be in the unit of mS/cm$^2$. This equation is used for the purpose of comparison between the classical model and the quantum model of cardiac membrane depolarization.

### *2.5. The mathematical formulation of a quantum synapse*

When a conducting cardiac fiber fires, there will be a slight increase in the extracellular concentration of potassium ions. These potassium ions can get the opportunity to tunnel through the closed gates of channels within the membrane of adjacent unstimulated conducting fibers. The probability of inducing an action potential in adjacent fibers can be calculated. The increase in the extracellular potassium concentration $[K]_{AP}$ per surface area unit from the propagation of a single action potential can be calculated by using the following equation:

$$[K]_{AP} = \frac{N_{AP}}{N_A V_E}, \quad (22)$$

where $N_{AP}$ is the number of potassium ions that exit to the extracellular compartment per surface area unit and per action potential, $N_A$ is Avogadro's number ( $6.02\times10^{23}$ mol$^{-1}$) and $V_E$ is the extracellular volume taken up by potassium ions as a result of diffusion during an action potential.
Another parameter that is considered in this context is the number of potassium ions hitting a single channel $N_K$, which can be calculated by using the following equation:

$$N_K = \frac{N_{AP}}{D^*}, \quad (23)$$

where $D^*$ is the number of ion channels per square micrometer of surface area.
Furthermore, to determine the relationship between the value of tunneling probability required to induce an ectopic action potential in an adjacent unstimulated cardiac fiber and the number of potassium ions hitting a single channel, the following equation can be used:

$$MC_{Na}[Na]_o + MC_K[K]_o + MC_{Q-K(o)}[\mathrm{K}]_{AP} = e^{-\frac{qV_m(\mathrm{Thr})}{K_B T}} (MC_{Na}[Na]_i + MC_K[K]_i), \quad (24)$$

where $V_{m(Thr)}$ is the value of membrane potential required to induce an action potential, which is assumed to be 0.055 V.
Based on Equations (22)–(24), the relationship between the threshold value for quantum tunneling and the number of potassium ions hitting a single potassium channel can be calculated by using the following equation after considering substituting the values in Equation (24):

$$2.71+3.88\times10^{-2}\times10^{8}\frac{N_K D^*}{N_A V_E}T_{Q(Thr)}=8.9\,, \tag{25}$$

where $3.88\times10^{-2}=\frac{q^2}{h}$, with a unit of mS ,and $10^8$ is the number of ion channels per square centimeter corresponding to 1 channel/$\mu m^2$ ( i.e., the minimum *D* value) to get a conductance by the unit of mS/cm$^2$.

Eventually, the threshold quantum tunneling probability can be calculated by using the following equation:

$$T_{Q(Thr)}=1.6\times10^{-6}\frac{N_A V_E}{N_K D^*}\,. \tag{26}$$

If we assume that $N_{AP}=1\times10^4$ potassium ions/$\mu m^2$ per single action potential, $V_E=1\mu m^3$ and $D^*=100$ channels/$\mu m^2$. Then, the corresponding increase in the extracellular potassium concentration surrounding 1 $\mu m^2$ surface area of cardiac fiber will be $[K]_{AP}=0.0166$ mmol/L. There are $N_K=10^2$ potassium ions per single channel, and the value of quantum tunneling required to depolarize the membrane potential to threshold value of 0.055 V is $T_{Q(Thr)}=9.63\times10^{-5}$. This means that a minimum fraction of $9.63\times10^{-5}$ of the total number of potassium ions hitting a channel is required to depolarize the membrane potential to the threshold value and induce an ectopic action potential. Accordingly, if at least one of the 100 potassium ions hitting the channel tunneled through the closed gate, then the fraction will be 0.01, which is higher than the threshold value for quantum tunneling. This means that the fraction of 0.01 (i.e., the tunneling of one potassium ion) is enough to induce an ectopic action potential via the process of quantum tunneling.

The task now is to calculate the probability of achieving the fraction of 0.01 based on the actual tunneling probability of potassium ions.

The Bernoulli trial equation can be employed to calculate the probability of action potential induction:

$$P(Z)=\frac{N!P^Z(1-P)^{N-Z}}{(N-Z)!Z!}\,, \tag{27}$$

where *N* is the number of trials available, *Z* is the number of successful trials desired from the total number, *P* is the probability of a successful trial and *P(Z)* is the probability of achieving a *Z* number of successful trials.

When *Z* = 0, Equation (27) becomes

$$P(0)=(1-P)^N\,. \tag{28}$$

Accordingly, the probability of obtaining at least one successful trial, $Z\geq1$, is calculated by solving $P(Z\geq1)=1-(1-P)^N$.

The probability that at least one potassium ion can tunnel through the closed gate and induce an action potential through a single channel in a surface area of $1\mu m^2$ can be calculated by using the following

equation:

$$P_1 = 1-(1-T_{Q-K})^{N_K}. \tag{29}$$

where $T_{Q-K}$ is the quantum tunneling probability of potassium ions.
Assuming that at least one ion channel from the total number $D$ is sufficient to depolarize the membrane potential to the threshold value, then the probability to induce an action potential in a surface area of $1\mu m^2$ can be calculated:

$$P_2 = 1-(1-P_1)^D. \tag{30}$$

Eventually, the probability of action potential induction in at least $1\mu m^2$ area from the total number of $1\mu m^2$ surface area units available for quantum tunneling of potassium ions can be calculated:

$$P_3 = 1-(1-P_2)^{N_{\mu m^2}}, \tag{31}$$

where $N_{\mu m^2}$ is the total number of $1\mu m^2$ surface area units of the membrane of cardiac cells available for the quantum tunneling of potassium ions.

## 3. Results

In this section, we present simulations of the quantum tunneling phenomenon, the quantum conductance and the quantum tunneling-induced membrane depolarization for a barrier height $G$ of $10^{-20}$ J and varying gate length $L$ values up to $5\times10^{-10}$ m, which is around the length of three hydrophobic residues. These values are consistent with those observed particularly, the experimental energy values were within the range of $10^{-20}$ J, which are kJ/mol = $0.17\times10^{-20}$ J or kcal/mol = $0.69\times10^{-20}$ J [30–32].

### *3.1. The quantum tunneling of ions and the quantum conductance*

Based on Equations (6) and (8), the quantum tunneling probability of potassium and sodium ions for the two potential barriers can be simulated. See Figure 6.

Based on Equation (9), the quantum unitary conductance for sodium and potassium channels for the two potential barriers can be simulated. See Figure 7.

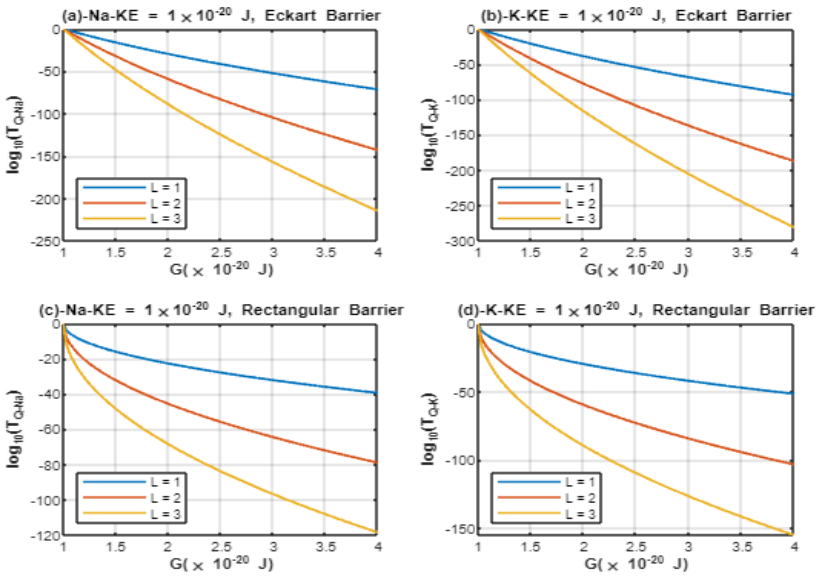


**Figure 6.** The relationship between the logarithm of the quantum tunneling probability and the barrier height of the closed gate $G$ for different values of gate length $L$ (the unit is $\times 10^{-10}$ m) and a kinetic energy $KE = 1 \times 10^{-20}$ J. Simulations of the quantum tunneling of sodium and potassium ions through the Eckart barrier are represented in (a) and (b), and through the rectangular barrier in (c) and (d).

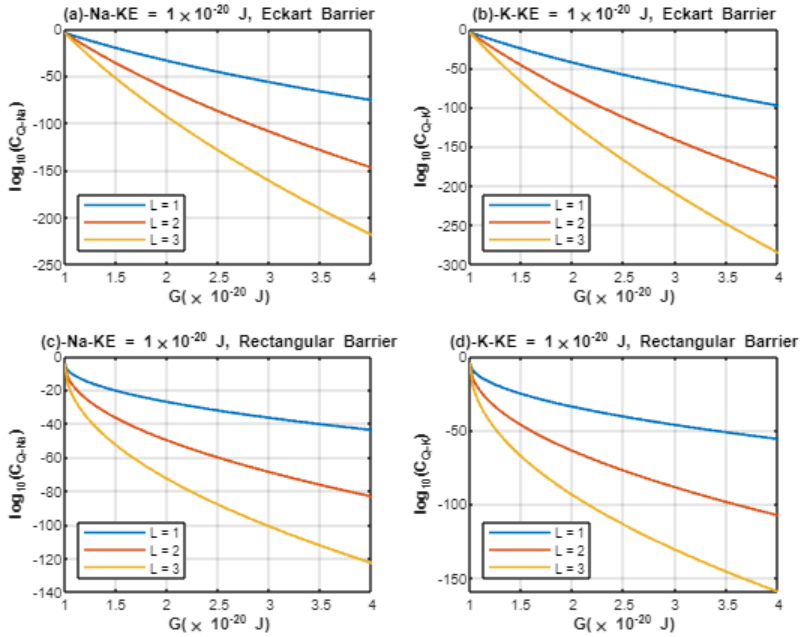


**Figure 7.** The relationship between the logarithm of the quantum unitary conductance and the barrier height of the closed gate $G$ for different values of gate length $L$ (the unit is $\times 10^{-10}$ m) and a kinetic energy $KE = 1 \times 10^{-20}$ J. The unit of quantum unitary conductance is (S). Simulations of the quantum unitary conductance of sodium and potassium ions through the Eckart barrier are represented in (a) and (b), and through the rectangular barrier in (c) and (d).

Based on Equation (10), the quantum membrane conductance of sodium and potassium ions for the two potential barriers can be simulated. See Figure 8.

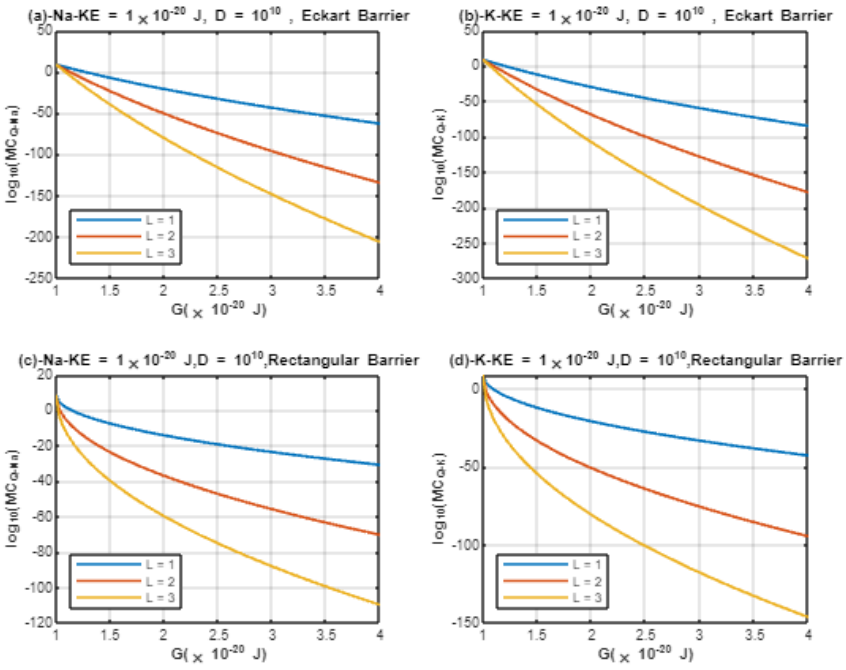


**Figure 8.** The relationship between the logarithm of the quantum membrane conductance and the barrier height of the closed gate $G$ for different values of gate length L (the unit is $\times 10^{-10}$ m), a kinetic energy $KE = 1 \times 10^{-20}$ J and a density of channels $D = 10^{10}$ channels/cm$^2$. The unit of quantum membrane conductance is mS/cm$^2$. Simulations of the quantum membrane conductance of sodium and potassium ions through the Eckart barrier are represented in (a) and (b), and through the rectangular barrier in (c) and (d).

### *3.2. The quantum tunneling-induced membrane depolarization*

As a result of the quantum tunneling of cations, it is expected that tunneling can generate an electric flow that can change the membrane potential according to the net direction of the tunneling flow. Based on Figure (6), it is clear that the tunneling probability for extracellular ions exceeds that for the intracellular ions. Therefore, a net inward current of positive ions will be generated and a depolarization is expected to occur. It is predicted that, as the barrier height G decreases, the tunneling probability is augmented and a depolarization occurs. Based on Equation (13), the influence of the drop in the barrier height on the membrane potential can be simulated. See Figure 9.

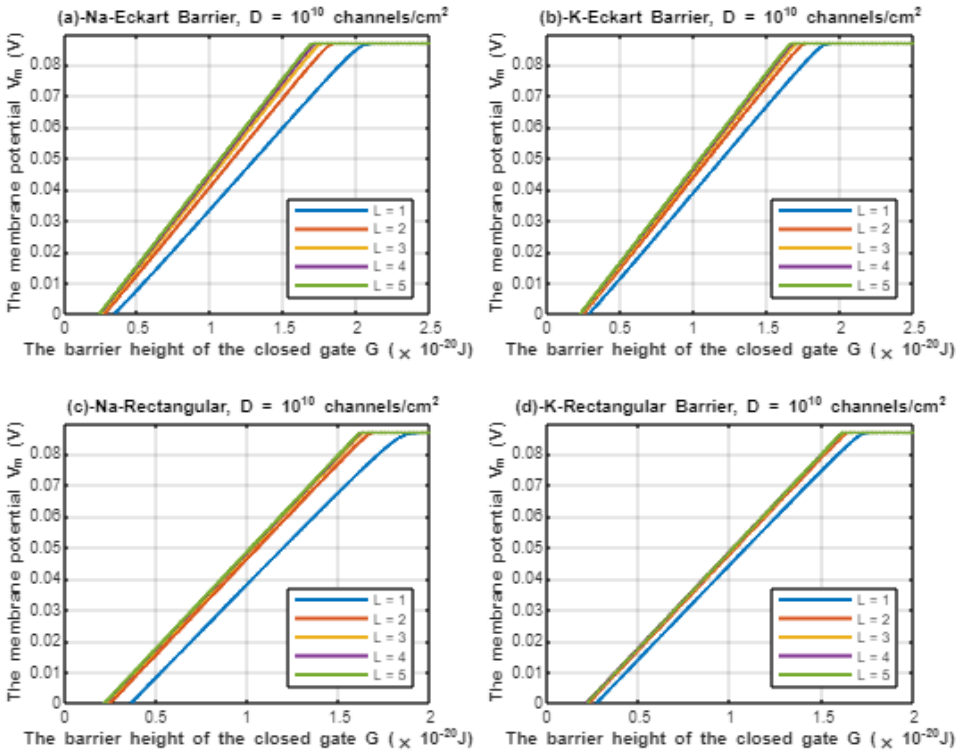


**Figure 9.** (a,b): The relationship between the membrane potential and the barrier height of the closed gate $G$ of the Eckart barrier for sodium and potassium ions is represented, respectively. (c,d): The relationship between the membrane potential and the barrier height of the closed gate G of the rectangular barrier for sodium and potassium ions is represented, respectively. The relationship is simulated for different values of gate length L (the unit is $\times 10^{-10}$ m) and $D = 10^{10}$ channels/cm$^2$.

### *3.3. The thermally assisted quantum tunneling-induced membrane depolarization*

The biological environment can provide the channel's gate with thermal energy, which can lower the energy barrier of the gate, thus enhancing the tunneling probability and predisposing the membrane potential for depolarization at higher values of barrier height $G$.

Based on Equations (17)–(19), extent to which the thermal energy influences quantum tunneling-induced membrane depolarization can be simulated. See Figures (10) and (11). In this investigation, the membrane potential, as a contributor to the kinetic energy of the ion, is assumed to be a variable. In other words, we assume that the process of tunneling, thermal energy transfer and process of partially dilating the pore to decrease the barrier height are slow enough to allow ions to be affected by the changes in the membrane potential. Accordingly, the membrane potential $V_m$ that is present in the mathematical expression of kinetic energy $KE$ and the expression $e^{\frac{-qV_m}{K_BT}}$ are both held as a variable to plot the Figures 10 and 11.

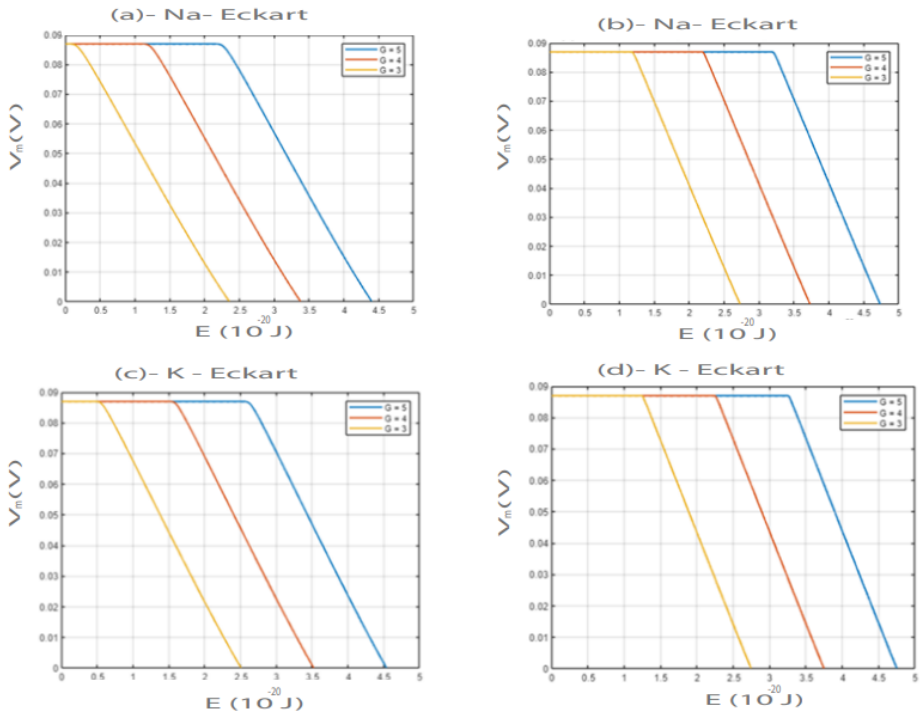


**Figure 10.** (a,b): The slow influence of the tunneling-assistive thermal energy on the membrane potential, as mediated by the quantum tunneling of sodium ions through the Eckart barrier is shown for $L = 1\times10^{-10}$ m and $L = 5\times10^{-10}$ m, respectively. (c,d): The slow influence of the tunneling-assistive thermal energy on the membrane potential, as mediated by the quantum tunneling of potassium ions through the Eckart barrier, shown for at $L = 1\times10^{-10}$ m and $L = 5\times10^{-10}$ m, respectively. The simulations were conducted by using $D = 10^{10}$ channels/cm$^2$ and three different values of G ($G = 5, G = 4, G = 3$) note that the values of $G$ are presented for $\times10^{-20}$ J.

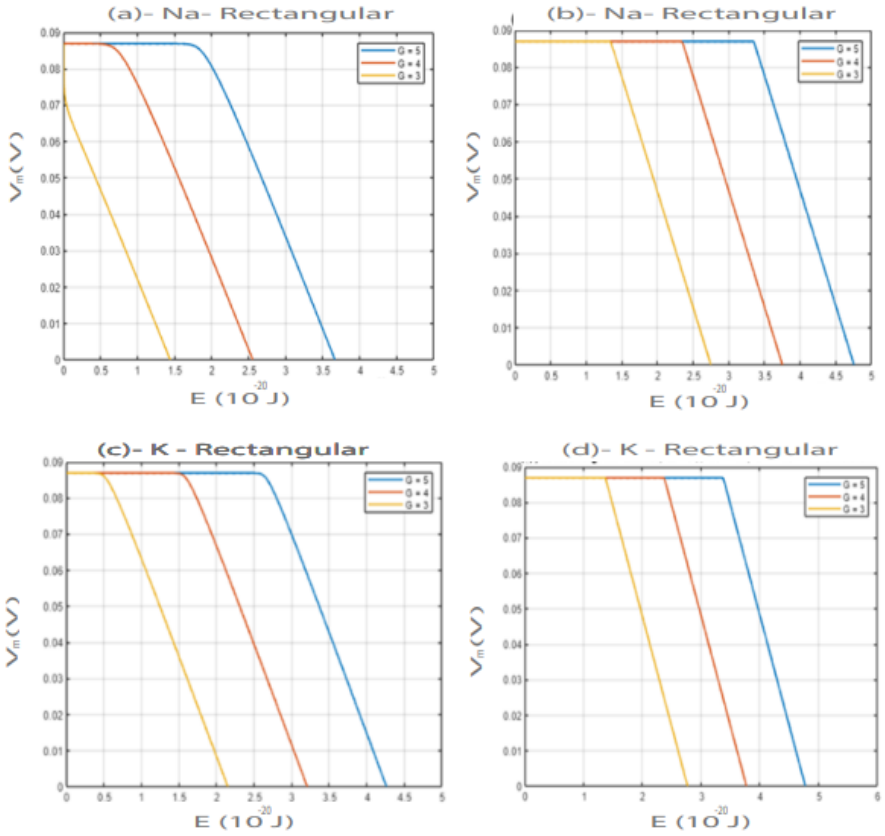


**Figure 11.** (a,b): The slow influence of the tunneling-assistive thermal energy on the membrane potential, as mediated by the quantum tunneling of sodium ions through the rectangular barrier, is shown for $L = 1\times10^{-10}$ m and $L = 5\times10^{-10}$ m, respectively. (c,d): The slow influence of the tunneling-assistive thermal energy on the membrane potential, as mediated by the quantum tunneling of potassium ions through the rectangular barrier, is shown for $L = 1\times10^{-10}$ m and $L = 5\times10^{-10}$ m, respectively. The simulations were conducted by using $D = 10^{10}$ channels/cm2 and three different values of $G$ ($G = 5, G = 4, G = 3$) note that the values of $G$ are presented for $\times10^{-20}$ J.

On the other hand, if the process of tunneling, thermal energy transfer and process of lowering the energy barrier height are fast enough to prevent ions from being affected by the changes in membrane potential, the initial membrane potential, which is 0.087 V in our study, will serve as the source of kinetic energy, and it can be assumed to be constant. In this case, the rapid depolarization to the threshold and thus inducing an action potential is faster than the process of ions being affected by the pre-action potential depolarization. Accordingly, the membrane potential $V_m$ that is present in the mathematical expression of kinetic energy $KE$ will be a constant, i.e., 0.087 V ,and the membrane potential $V_m$ in the expression $e^{\frac{-qV_m}{K_B T}}$ is a variable plotted in Figures 12 and 13.

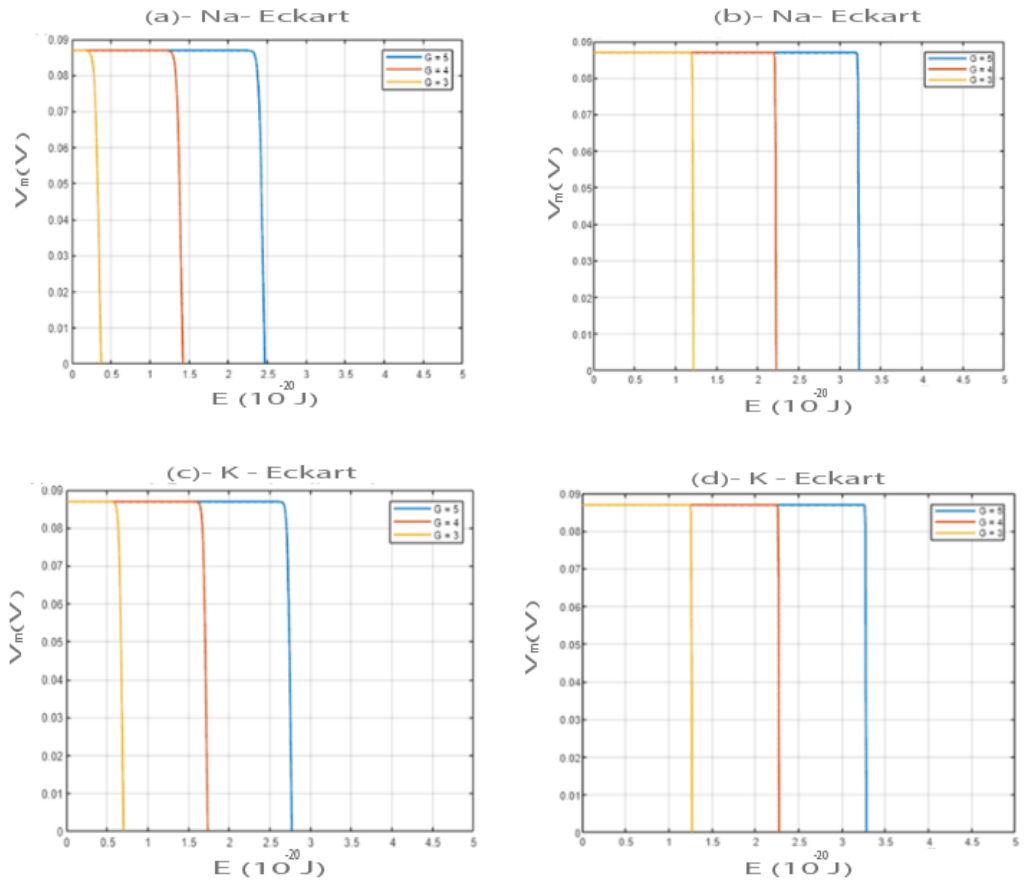


**Figure 12.** (a,b): The fast influence of the tunneling-assistive thermal energy on the membrane potential, as mediated by the quantum tunneling of sodium ions through the Eckart barrier , is shown for $L = 1\times10^{-10}$ m and $L = 5\times10^{-10}$ m, respectively. (c,d): The fast influence of the tunneling-assistive thermal energy on the membrane potential , as mediated by the quantum tunneling of potassium ions through the Eckart barrier, is shown for $L = 1\times10^{-10}$ m and $L = 5\times10^{-10}$ m, respectively. The simulations were conducted by using $D = 10^{8}$ channels/cm$^2$ , $V_{m(initial)} = 0.087$ V and three different values of $G$ ($G = 5, G = 4, G = 3$), note that the values of G are presented for $\times10^{-20}$ J.

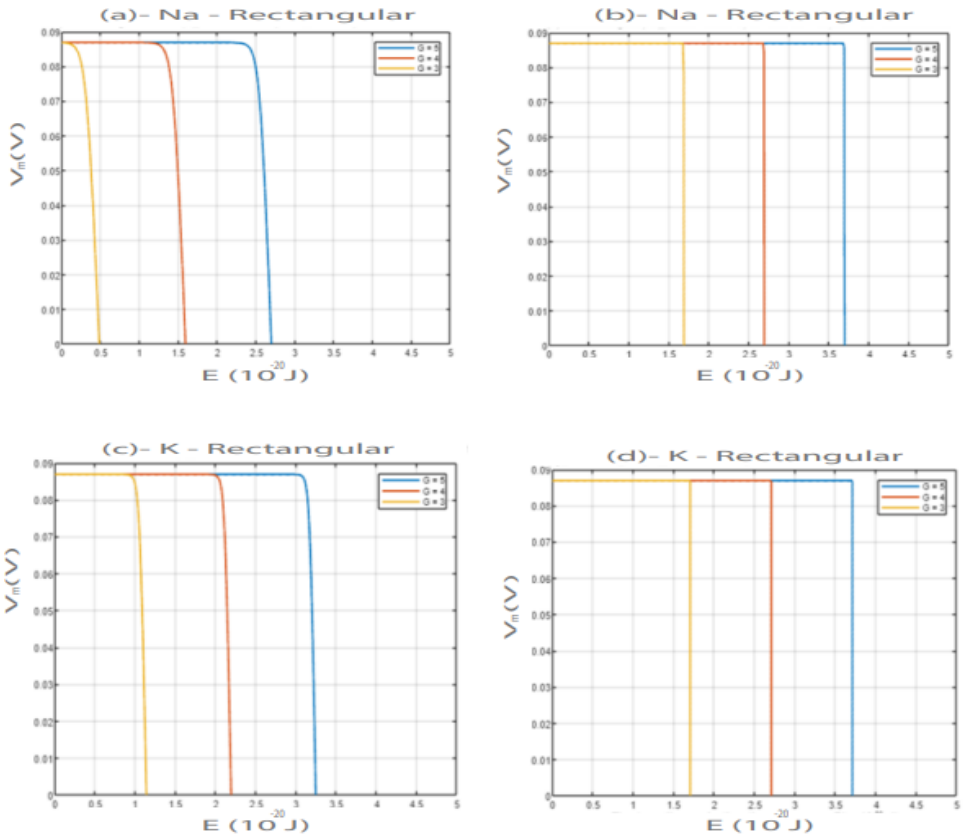


**Figure 13.** (a,b): The fast influence of the tunneling-assistive thermal energy on the membrane potential for potassium ions through the rectangular barrier, is shown for $L = 1\times10^{-10}$ m and $L = 5\times10^{-10}$ m, respectively. (c,d): The fast influence of the tunneling-assistive thermal energy on the membrane potential for potassium ions through the rectangular barrier, is shown for $L = 1\times10^{-10}$ m and $L = 5\times10^{-10}$ m, respectively. The simulations were conducted by using $D = 10^8$ channels/cm$^2$, $V_{m(initial)} = 0.087$ V and three different values of $G$ ($G = 5, G = 4, G = 3$) note that the values of G are presented for $\times10^{-20}$ J.

We performed the previous analysis by using $D = 10^8$ channels/cm$^2$, which is the minimum value for $D$ used in this study, to exhibit the low sensitivity of the tunneling-induced depolarization to the number of channels, especially if it is compared with the classical model, as will be shown in the next section.

### *3.4. The influence of the classical opening of voltage-gated channels on the membrane potential*

To show the ability of the quantum tunneling model to change the membrane potential, we simulated the influence of the classical opening of sodium and potassium channels on the membrane potential by using Equation (21). See Figure 14.

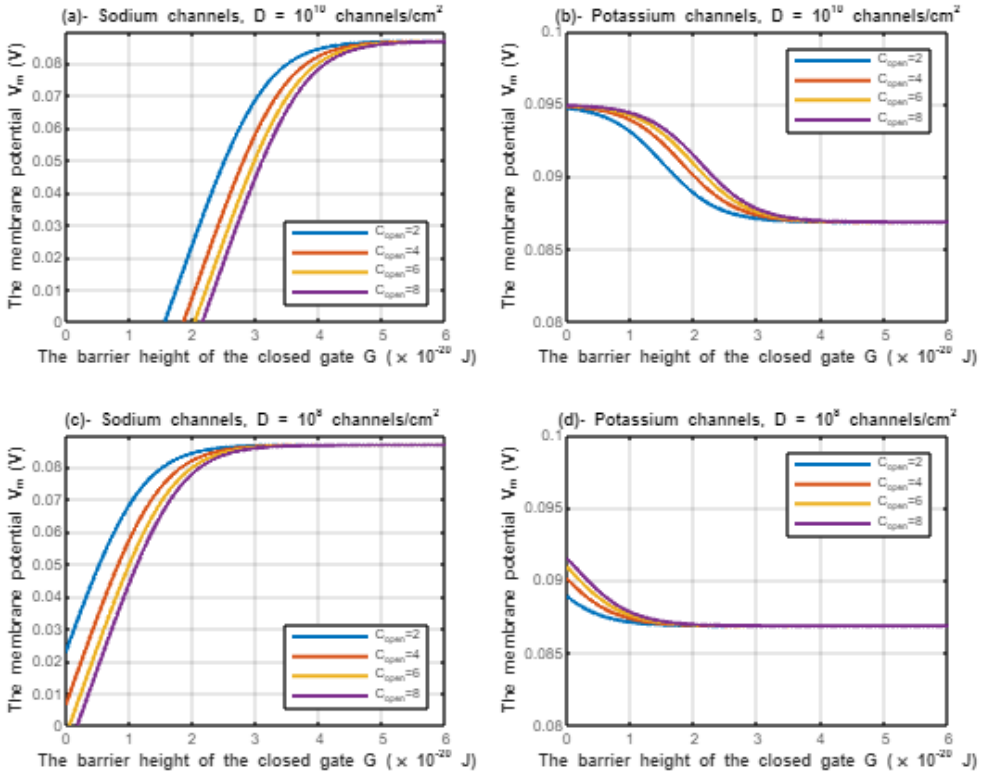


**Figure 14.** (a,b): The relationship between the barrier height of the closed gate $G$ and the membrane potential due to the opening of sodium and potassium channels is represented, respectively. The simulations were conducted by using different values of single channel conductance and $D = 10^{10}$ channels/cm$^2$. (c,d): The relationship between the barrier height of the closed gate $G$ and the membrane potential due to the opening of sodium and potassium channels is represented, respectively. The simulations were conducted by using different values of single channel conductance and $D = 10^{8}$ channels/cm$^2$. The unit of $C_{open}$ is $10^{-9}$ mS.

### *3.5. The ectopic action potentials induced by the quantum synapse*

According to Equations (29)–(31), the probability of inducing an ectopic action potential along the surface area of unstimulated cardiac fibers when an adjacent stimulated fiber fires can be evaluated. See Figure 15. The analysis was performed with the following values: the initial membrane potential $V_m = 0.087$ V, the number of potassium ions hitting a single channel $N_K = 100$, the density of channels $D = 10^2$ channels/ $\mu m^2$ and the number of $1\mu m^2$ area $N_{\mu m^2} = 100$. This type of communication between cardiac fibers will be coined in this paper to be a 'quantum synapse', in which two fibers can communicate without any anatomical connection or an electrical connection like a gap junction.

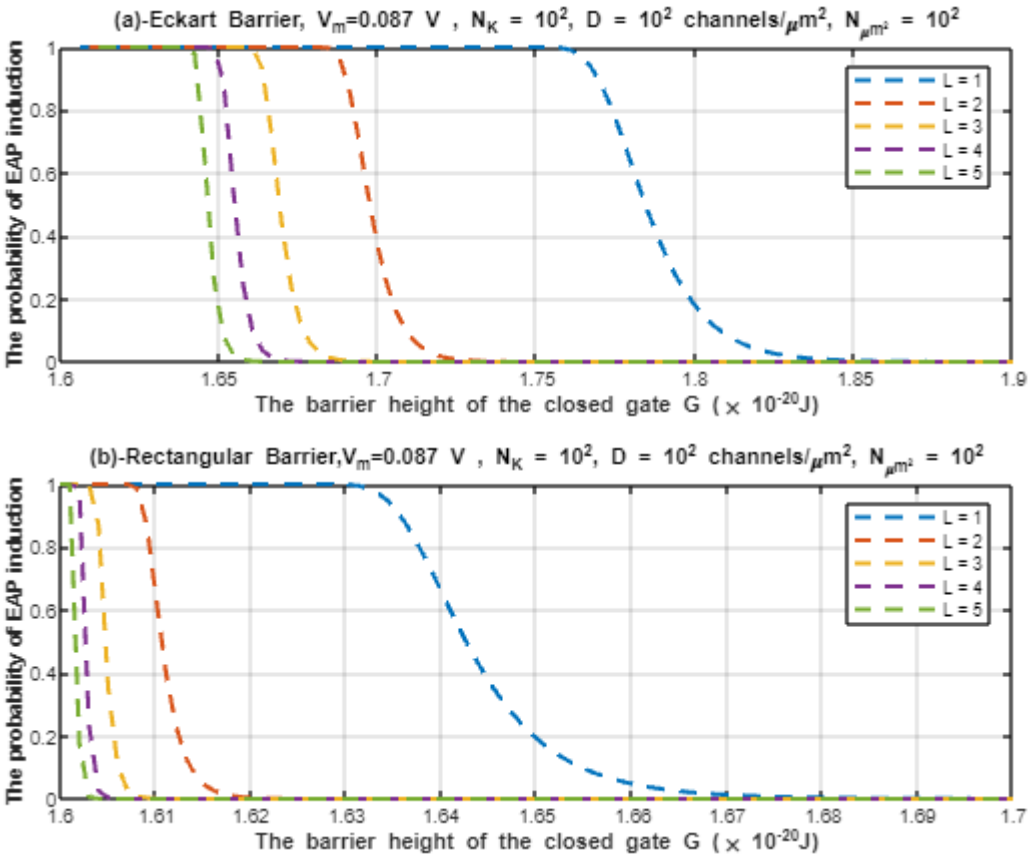


**Figure 15.** (a,b): The relationship between the barrier height of the closed gate *G* and the probability of inducing an ectopic action potential at different values of gate length for the Eckart barrier and rectangular barrier is represented, respectively. The relationship is plotted according to the values above each figure.

## 4. Discussion

### *4.1. Overview of the quantum tunneling model of ions*

Three major pathological mechanisms contribute to the pathogenesis of cardiac arrhythmias. These include depolarization-induced automaticity, triggered activity due to afterdepolarization and the formation of a reentry circuit. To the best of the authors' knowledge, all of these mechanisms were investigated from a classical perspective by using classical mechanics. However, the role of the quantum behavior of ions in the pathogenesis of cardiac arrhythmias has not yet been investigated adequately. This study is a continuation of previous studies [48,49] that focused on the quantum behavior of ions in the context of cardiac arrhythmias. The function of tunneling is to allow particles to pass through classically impermeable barriers via their quantum wave behavior. In the context of ion channels, it allows ions to pass through the closed gates. Hence, quantum conductance can be calculated and the influence of quantum tunneling on the excitability of cells can be investigated.

The necessity of quantum tunneling stems from the ability of this phenomenon to explain the transport of particles, such as ions, through barriers that have higher energy than the particles themselves. In the context of ion channels, their closed gates represent barriers that classically block

the permeation of ions. Hence, utilizing the mathematics of quantum tunneling allows researchers to investigate and explore the characteristics of transport that is not allowed classically. Moreover, the quantum behavior of particles within biological systems, including electrons, protons, ions and even large organic molecules has been shown to be necessary to explain and understand several physiological and pathological conditions, such as photosynthesis, enzymatic reactions and DNA point mutations [23,24]. Accordingly, exploring the quantum behavior of ions is as necessary as the classical behavior. This will help researchers to obtain additional insights into the pathophysiological mechanisms related to the function of ion channels, as associated with cardiac arrhythmias.

The quantum tunneling of ions implies that they have a non-zero probability of passing through a gate that is classically closed since its energy barrier height is higher than the energy of the ions. The quantum tunneling process is affected by the shape of the barrier; hence, we chose two possible shapes to explore how they can influence the tunneling probability. The closed gate of voltage-gated channels is composed of hydrophobic residues that form a narrow pore, which forms a potential energy barrier. This has been experimentally proved by using the PMFs for hydrophobic residues, materials and membranes [30,33,34,39–41]. The quantum tunneling is affected by the barrier height of the closed gate, the length of the gate, the kinetic energy and the mass of the ion. The secondary outcomes of the quantum tunneling are the quantum unitary conductance and the quantum membrane conductance. These are the quantities that determine the effects of the quantum tunneling on the membrane potential and the excitability of cardiac cells.

Based on our results represented in Figures (6)–(8), the quantum tunneling probability and quantum conductance stay within a range of insignificant values until the barrier height decreases to a critical value, at which they become significant and comparable to the values that can affect the membrane potential. Generally, they become significant once the barrier height value drops to less than $2\times10^{-20}$ J. However, this critical value varies according to the length of the gate, the mass and kinetic energy of the ion and the shape of the barrier. As the length of the gate and the mass of the ion increase, the critical value of *G* at which tunneling becomes significant decreases. This means that a larger drop in the barrier height is required to enhance the quantum tunneling of ions. Hence, the values of *G* at which the tunneling of sodium becomes significant are higher than those associated with the tunneling of potassium. On the other hand, as the kinetic energy of the ions increases, the critical value of *G* at which tunneling becomes significant increases, and vice versa.

### *4.2. The quantum tunneling-induced membrane depolarization*

In healthy cardiomyocytes, an energy barrier higher than $2\times10^{-20}$ J will guarantee a lower tunneling probability and, thus, a low quantum conductance that cannot affect the membrane potential. This can be observed in Figure 9, in which no change in membrane potential at higher energy barrier values can be noticed, and it is indicated by the plateau at the original resting membrane potential of 0.087 V. According to the results, it is clear that the quantum tunneling probability for extracellular ions is higher than the probability for intracellular ions due to the higher kinetic energy of extracellular ions. Thus, a net inward quantum current is expected to occur. Consequently, a membrane depolarization can be induced.

Membrane depolarization is the pathological trigger for automaticity and activity triggered by afterdepolarization. Based on the overview of the model of the quantum tunneling of ions, it was

predicted that the net inward tunneling flow of cations would depolarize the membrane potential. According to Figure 9, both sodium and potassium ions can depolarize the membrane potential via quantum tunneling under the conditions of both barrier shapes. However, the degree of depolarization by sodium ions is higher than that by potassium ions, mainly due to the mass difference, whereas the higher extracellular sodium concentration contributes minimally to such discrepancy. In addition, the quantum tunneling-induced membrane depolarization occurs at higher values of gate length i.e., up to $5\times10^{-10}$ m in our study. Furthermore, as the length of the gate increases, the difference in the degree of membrane depolarization with respect to the barrier height decreases as shown in Figure 9. This observation is clearer in the case of the quantum tunneling of potassium ions due to their larger mass.

Generally, the membrane depolarization starts when the barrier height $G$ decreases below $2\times10^{-20}$ J for both ions and both barriers. Otherwise, the quantum tunneling of ions has no influence on the membrane potential because, in this case, the quantum conductance is not significant or comparable to the classical conductance. Besides, Figure 9 shows that, as the barrier height $G$ decreases to below $2\times10^{-20}$ J, the quantum tunneling of both types of ions through the Eckart barrier becomes more likely to induce a higher degree of membrane depolarization than the rectangular barrier.

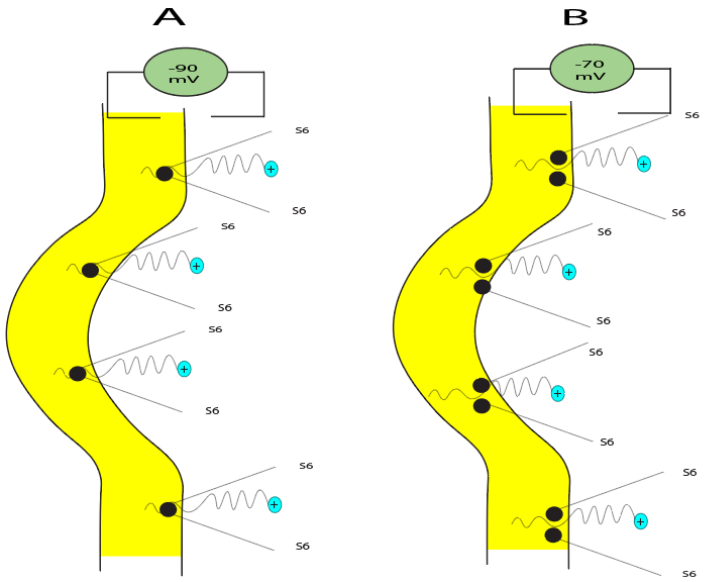


**Figure 16.** A schematic diagram which represents that quantum tunneling is too weak to influence the membrane potential when the barrier height of the gate is high, this is represented as occluded pores, or by a black dot, as illustrated in the fiber (A). In the state (B), there is quantum tunneling-induced membrane depolarization when there is a decrease in the barrier height of the closed gate, which is represented as a partially opened pore via two black dots that are separated from each other. The curve of the two cardiac fibers is purposed to indicate a pathology that affects the integrity of the membrane.

The quantum tunneling-induced membrane depolarization is schematically represented in Figure 16. The critical condition that should be present for the quantum tunneling-induced depolarization to

be apparent is the drop in the barrier height of the closed gate. This drop is associated with the same factors that predispose cardiac cells to arrhythmias. These include hypoxia, ischemia, infarction, acidosis, channelopathies, mechanical stretch or dilation or any cause that harms the integrity of the cellular membrane or ion channels themselves [16–18]. These risk factors are clearly found in the patients of intensive care units. The percentages of sodium and potassium ions necessary to find an abnormality in ion channels depends on the degree of the disruption of the hydrophobic interactions between the residues that form the gates of channels. This disruption increases as the presence of the pathological factors increases [30–34]. These pathological factors affect the integrity of the cellular membrane and the molecular structure of the channels themselves. Therefore, as the disruption in the hydrophobic interactions increases, the likelihood of finding an abnormality increases. Hence, the percentage may range from zero to 100% according to the degree of the hydrophobic disruption.

The induced depolarization due to these factors can be understood from the perspective of the classical and quantum models. The drop in the barrier energy increases the inward cationic flow. However, there are distinctive features of the quantum model that make it more advantageous than the classical model in terms of the voltage-gated channels. These features are thus described. 1) The quantum tunneling implies continuous and persistent flow of cations through the gate, while the classical model operates in the on-off or the open-closed system, which means that channels are not always available for the permeation of ions, and this depends on the probability of opening according to the Boltzmann distribution. Therefore, the quantum tunneling model ensures that membrane depolarization is present for a longer duration than the classical model, in which depolarization is canceled once open channels are inactivated or the activation gate becomes closed. 2) According to the quantum tunneling model, when there is a reduction in the barrier height, the sodium and potassium ions will be boosted to flow to the inside of the cell, but according to the classical model, the flow of sodium ions will be augmented to the inside and the flow of potassium ions to the outside. Therefore, the degree of depolarization will be higher in the case of the quantum tunneling model. As a result, the quantum behavior of ions contributes to the depolarization-induced automaticity more significantly than the classical behavior in terms of the degree and the duration of depolarization.

### *4.3. The thermally assisted quantum tunneling-induced membrane depolarization*

Furthermore, even at barrier height $G$ values higher than $2\times10^{-20}$ J, the quantum tunneling of ions can depolarize the membrane potential if the thermal energy of the biological environment is included as according to Equations (17)–(19). In this case, and according to the Boltzmann distribution, ion channels can be provided by an energy from the thermal biological system in a probabilistic manner. Thus, the provided thermal energy can lower the barrier height and, hence, the quantum tunneling of ions will be enhanced. As a consequence, it is expected that depolarization can occur at higher values than $2\times10^{-20}$ J, which is represented in Figures 10 and 11. According to these figures, quantum tunneling-induced membrane depolarization can occur at $G$ values of $3\times10^{-20}$ J, $4\times10^{-20}$ J and $5\times10^{-20}$ J for both barriers and gate lengths of $1\times10^{-10}$ m and $5\times10^{-10}$ m. Interestingly, the results show that the thermal energy does not need to be equivalent to or higher than the barrier height $G$ for the quantum tunneling to change the membrane potential. However, the classical model requires that the thermal energy provided should be equivalent to or higher than the barrier height for the classical transport to be influential enough to affect the membrane potential. This is another distinction between the two models, which implies that the depolarization by the quantum tunneling is more energetically

favorable than the classical transport of ions. Additionally, the thermal energy requirement for potassium ions to induce depolarization is higher than that for sodium ions at the same values of barrier height $G$ and gate length $L$. Moreover, as the gate length increases, the thermal energy requirement to depolarize the membrane potential increases.

The membrane depolarization reduces the barrier height of the closed gate according to the following equation [50]:

$$G = q_{gate}(V_m - V_{1/2}), \tag{32}$$

where $q_{gate}$ is the gating charge, $V_m$ is the membrane potential and $V_{1/2}$ is the half-activation voltage at which half of the channels are open.

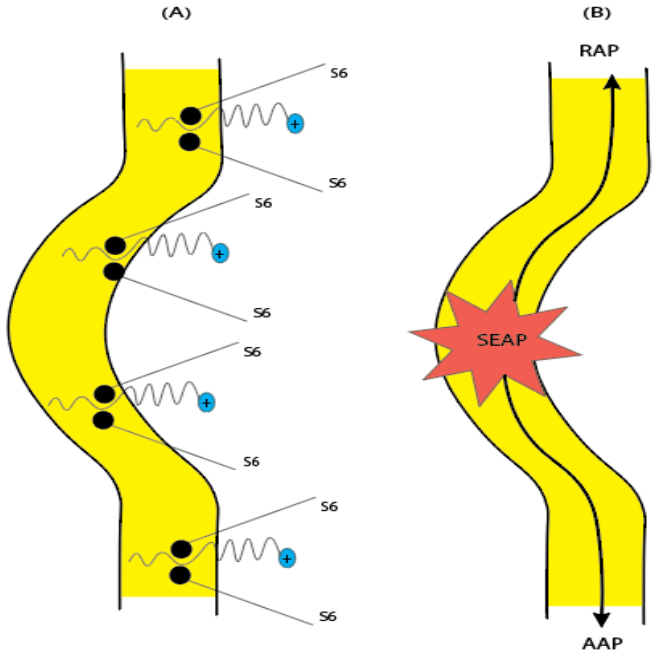


**Figure 17.** A schematic diagram showing that the quantum tunneling of cations in a conducting fiber (A) can induce a spontaneous ectopic action potential (SEAP) from which retrograde (RAP) and anterograde (AAP) action potentials are generated in the cardiac fiber (B). The curve of the two cardiac fibers is purposed to indicate a pathology that affects the integrity of the membrane.

The reduction in the barrier height as a result of membrane depolarization is due to the decrease in the difference between the resting membrane potential and the half-activation voltage; thus, a lower energy barrier is required for the ion channel to open. As a result, the cardiac cells are more readily stimulated by an external stimulus such as mechanical stretch, sympathetic stimulation, pressure, shear force, drugs and others. However, another mechanism that contributes to the pathogenesis of arrhythmias is the spontaneous firing of cardiac cells in the absence of any stimulus or trigger apart from the biological thermal environment. According to Figures 12 and 13, the quantum model predicts that the quantum tunneling of ions can induce a spontaneous ectopic action potential (SEAP) in the

absence of any external stimulus, except for the thermal energy as a part of the biological system. See Figure 17.

According to Figures 12 and 13 and under the condition of an initial membrane potential of 0.087 V, the thermally assisted quantum tunneling can induce sharp and acute changes in the membrane potential requiring lower cost of the thermal energy. This indicates that a small amount of thermal energy compared to the barrier height can depolarize the membrane potential to the threshold to induce a spontaneous action potential. According to the quantum model, cardiac cells have the potential to trigger a spontaneous action potential at every value of barrier height *G*, unlike the classical model, which is restricted by certain values of barrier height *G* and the number of ion channels *D*, as represented in Figure 14. In addition, the quantum model mandates that the thermal energy cost increases as the length of the gate increases, but without exceeding or even reaching the barrier height *G*. Moreover, according to the classical model, the depolarization to the threshold and subsequent induction of spontaneous action potential is not energetically favorable, because a thermal energy equivalent to or higher than the barrier height is required to reach the threshold, as represented in Figure 14. A numerical example will be given to elucidate such a difference between the two models. In Figure 12a, the quantum tunneling of sodium ions can depolarize the membrane potential to the threshold by acquiring a thermal energy of around $E = 1.5\times10^{-20}$ J for $G = 4\times10^{-20}$ J, $L = 1\times10^{-10}$ m and $D = 10^{8}$ channels/cm$^2$. This means that only 38% of the barrier height value G is required to trigger a spontaneous action potential. On the other hand, in Figure 14a, for $G = 4\times10^{-20}$ J, the classical opening of sodium channels cannot depolarize the membrane potential to the threshold for all of the different values of single -channel conductance and $D = 10^{10}$ channels/cm$^2$. Furthermore, the depolarization will be much weaker when the value of *D* drops to $10^{8}$ channels/cm$^2$, as in Figure 14c. However, the classical opening of sodium channels can trigger a spontaneous action potential when the barrier height G decreases to $3\times10^{-20}$ J or less for $D = 10^{10}$ channels/cm$^2$ ,and around $1.5\times10^{-20}$ J or less for $D = 10^{8}$ channels/cm$^2$.This implies that channels must have a thermal energy that is that is equivalent to or higher than the barrier height for the channels to open and the spontaneous action potential to be triggered. However, this means that 100% of the *G* value or higher is required to depolarize the membrane potential to the threshold via the classical opening of channels. This emphasizes the difference between the two models, which was mentioned earlier, i.e., that the quantum tunneling is more energetically favorable than the classical transport and thus better equipped to depolarize the membrane potential and induce an action potential.

Besides, in Figure 14b, it is clear that the classical opening of potassium channels results in membrane hyperpolarization above 0.087 V, which is what is expected according to the classical model. However, if this figure is compared with Figures 12 and 13, it is obvious that potassium ions induce membrane depolarization instead of hyperpolarization. This is another major distinction between the two models, as we mentioned earlier. In this case, the quantum tunneling of both the sodium and potassium ions contributes to the depolarization and the spontaneous firing instead of only sodium ions, which are opposed by potassium ions in the case of the classical model.

Afterdepolarization, especially the EAD, occurs when there is a shift in the cationic current toward the inward direction [10,11], and .as it was explained earlier, the quantum tunneling of ions enhances the inward cationic current quantitatively and qualitatively. The quantitative enhancement is mediated by the tunneling inflow of both sodium and potassium ions, and the qualitative enhancement is mediated by the low energy cost required to increase the tunneling passage of ions. Moreover, the higher tendency of membrane depolarization, as mediated by the quantum tunneling of ions, can explain the higher proneness of the critical patients to cardiac arrest, where most of the sodium

channels are inactivated due to a high degree of depolarization. According to the thermally assisted quantum tunneling, even healthy cardiomyocytes with higher values of energy barrier can trigger a membrane depolarization, but this is expected to occur with a low frequency, as thermal energy cost will be higher than the energy cost for unhealthy cardiomyocytes with lower energy barrier values.

### *4.4. The formation of the quantum synapse and the reentry circuit*

According to the quantum tunneling model, the firing of one cardiac fiber can trigger an action potential in an adjacent unstimulated cardiac fiber via the quantum tunneling of potassium ions that exit to the extracellular fluid during the firing of the stimulated fiber. The unique aspect in this communication is that the interaction is not mediated by any anatomical connection or, even an electrical one, such as a gap junction. Thus, we coin this type of synapse to be a quantum synapse. See Figure 18.

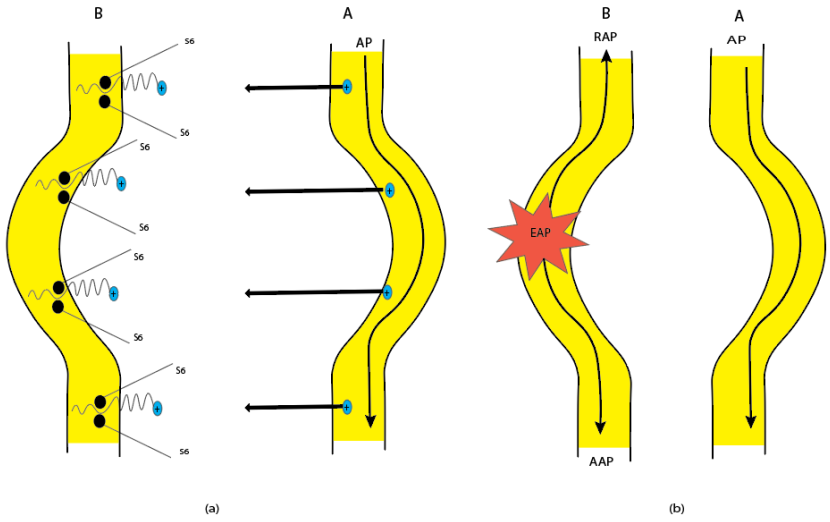


**Figure 18.** A schematic diagram of the quantum synapse formation. (a): When fiber (A) initiates an action potential, there will be an increase in the extracellular potassium concentration. These potassium ions will get the chance to tunnel through the closed channels in the membrane of the adjacent unstimulated fiber (B). (b): Eventually, an ectopic action potential (EAP) will be elicited at some point along the fiber (B). The EAP will generate a retrograde action potential (RAP) and an anterograde action potential (AAP). The curve of the two cardiac fibers is purposed to indicate a pathology that affects the integrity of the membrane.

The firing of a cardiac fiber will result in the outflow of potassium ions. This will increase the extracellular potassium concentration around the adjacent unstimulated cardiac fibers. These potassium ions will get the opportunity to tunnel through the closed channels in the membranes of neighboring fibers. As we explained earlier, potassium ions can depolarize the membrane potential. Hence, there is a probability that they can depolarize the membrane potential to the threshold at some point along the surface area of the unstimulated fibers. This will result in ectopic action potential induction, and retrograde and anterograde action potentials will be generated.

The probability of inducing an ectopic action potential via a quantum synapse is represented in Figure 15 for both barriers and at different values of gate length. This probability increases as the barrier height *G* value decreases, and as the length of the gate decreases. As we mentioned earlier, the drop in the barrier height of the gate occurs under the same pathological conditions that predispose the cardiac tissue to tachyarrhythmias. The probability of ectopic action potential induction is higher when the quantum tunneling of potassium ions occurs through the Eckart barrier. This is due to the small values of G at which the quantum synapse is formed. The small values of G ensures that the area under the curve for the Eckart barrier is smaller than that for the rectangular barrier; thus, there is higher tunneling probability for the Eckart barrier.

The classical model of a reentry circuit mandates that the two fibers must be connected proximally and distally for the circuit to be formed. However, the quantum tunneling model can explain the reentry without the requirement of the proximal and distal anatomical connection. It can explain the reentry because, once an ectopic action potential is formed at some point on an unstimulated fiber, retrograde and anterograde action potentials will be formed. The retrograde action potential will be transmitted in the opposite direction of the usual action potential, and it will stimulate the cardiac tissue above to reach the original site, which sends more impulses anterogradely, and the anterograde action potential will be transmitted to the cardiac tissue below to augment the anterograde impulses. Thus, tachyarrhythmias are expected to be triggered. Additionally, even the spontaneous ectopic action potentials induced by the quantum tunneling can form a 'half-reentry circuit' in which the ectopic action potential can transmit anterograde and retrograde action potentials, resulting in the reentry of impulses retrogradely to the site of origin, however, we coin the term as half-circuit because, in this case, one fiber alone generates anterograde and retrograde action potentials, instead of two fibers. See Figure 18.

Another feature that distinguishes both models is that the quantum model is less dependent on the refractory period duration and the conduction velocity. In other words, according to the classical model, if the impulse reaches the fiber while it is in the refractory period, the reentry circuit will be blocked, while the quantum model deals with the success of the reentry in a probabilistic way, as it is represented mathematically in Equations (29)–(31). and, graphically, in Figure 15. This adds another distinction between the two models, which is the likelihood of the reentry to be formed. The likelihood of success in the quantum model is higher than that for classical model since the success rate is a spectrum from 0 to 1, while it is either 0 or 1 according to the classical model. Additionally, during the relative refractory period, the voltage-gated potassium channels open in response to the depolarized membrane potential to repolarize it back to normal. This membrane depolarization decreases the barrier height of the closed gate of potassium channels thus, augmenting the tunneling probability and increasing the probability of an ectopic action potential, even when the fiber is in the refractory period.

In summary, the classical model mediates the reentry circuit when there is anatomical connection proximally and distally, while the quantum model predicts the formation of the reentry circuit either by quantum synapse or spontaneous ectopic action potential formation. See Figure 19.

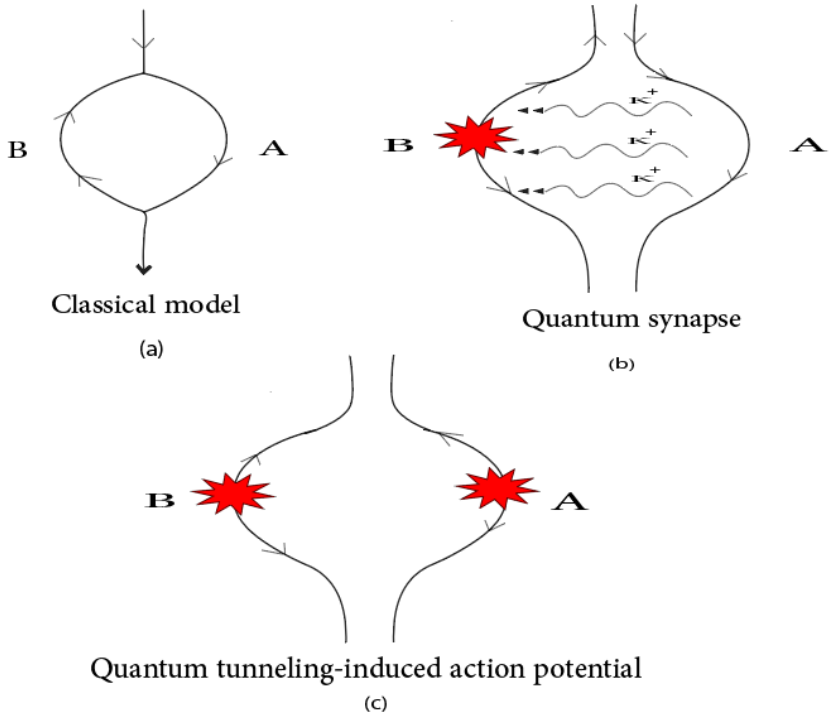


**Figure 19.** A schematic representation that compares the two models in terms of the reentry circuit formation. (a): The classical model states that the reentry circuit is formed when there is anatomical connection at the proximal and the distal ends. (b): The circuit is formed via the quantum synapse mediated by the quantum tunneling of potassium ions. (c): The spontaneous firing in each fiber can form a half-circuit in which each fiber generates retrograde and anterograde action potentials that are independent from each other.

### *4.5. The distinctive features of the present model*

Our present model has several improvements and features that distinguish it from those of previous studies that focused on cardiac arrhythmias from a quantum mechanical perspective [48,49]. These features are as follows 1) The present study involved both sodium and potassium ions in the simulations and compared them in terms of the quantum conductance and membrane depolarization of cardiac cells. 2) The present study focused on the influence of changing the barrier shape on the quantum tunneling probability of ions. 3) The present study revisited the underlying mechanism of a reentry circuit by applying the idea of the quantum synapse that is mediated by the quantum tunneling of potassium ions. 4) The present study introduced two ways in which the thermal biological environment can influence the membrane potential of cardiac cells. These are referred to as slow and fast influences; the slow influence can serve to explain the depolarization-induced automaticity and afterdepolarization, and the fast influence can serve to explain the spontaneous action potential and the formation of anterograde and retrograde action potentials. 5) The present study has shown mathematically that the arrhythmogenic process mediated by the quantum tunneling of ions is more energetically favorable than the classical transport of ions.

*4.6. How the quantum tunneling of ions can be validated*

Ion channels have received considerable attention from quantum biologists in recent years. They focused on applying the mathematics of quantum mechanics to ions within the selectivity filter (SF), which is the part that is responsible for determining the discrimination between ions and makes the ion channel selective for a specific ion [51–53]. These works [51–53] set the theoretical basis for the quantum behavior of ions in the SF, and they explained the two major characteristics of an SF via the quantum coherence and quantum non-locality principle. These two characteristics are the high conduction rate of ions and the high selectivity toward specific ions. Interestingly, an experimental model called the terahertz (THz) trapped ion model, was used recently to validate and prove the existence of the quantum tunneling of potassium ions through the potential energy barriers of the SF [54]. Briefly, this model uses THz-level electromagnetic radiation to trap ions at the zero-point energy, which means that the quantum number of the energy level equals zero. This allows researchers to investigate the tunneling effect on the ion permeation and the kinetic energy requirement to cross the barrier. Interestingly, the authors of the same paper extended their work for future experiments, proposing, theoretically, two experimental approaches including THz resonance fluorescence and the intense field non-resonant effect to detect the rapid quantum transport. These methods are expected to sustain the quantum coherence of ions without collapsing the wave function or eliminating the quantum tunneling effect. Therefore, the classical methods, including patch-clamp measurements, ion-sensitive electrodes and fluorescence-based assays, are more likely to collapse the quantum behavior of ions, and are thus less reliable methods for the detection of the rapid quantum transport. Hence, one is less likely to notice obvious quantum effects by using the classical methods.

To the best of the authors' knowledge, quantum biologists have not studied the quantum behavior of ions. neither theoretically nor experimentally within the intracellular hydrophobic gate, except in our previous work, which addressed the mathematical modeling of tunneling ions [28]. Therefore, there are no experimental studies until now that have proved the quantum tunneling effect within the intracellular gate. However, the THz trapped ion model was applied to ions within the SF [54]; hence, it can be applied to the hydrophobic gate, because both of them (the hydrophobic gate and the SF) form a potential energy barrier that resists the passage of ions. Moreover, we expect that applying the THz model to the closed gate will be easier since it forms one potential barrier instead of four consecutive barriers as with the SF [54]. Therefore, the experimental results obtained for SF [54] can be extrapolated and applied to the hydrophobic gate. Here, we will mention how our theoretical results are consistent with the experimental observations that were obtained for the SF. This will provide a huge motivation to apply the THz trapped ion model to validate our mathematical model of the quantum tunneling of ions through the closed gate. According to the THz trapped ion model, the tunneling effect will increase the rate of permeation and decrease the kinetic energy requirement of potassium ions to cross the barrier [54]. These are the same conclusions inferred from the present work. As the barrier height of the closed gate decreases below $2\times10^{-20}$ J, the quantum unitary conductance approaches of its maximum value of $\frac{q^2}{h}=3.88\times10^{-5}$ S, which is graphically represented in Figure 7. On the other hand, the classical opening of ion channels results in conductance values within the magnitude of $10^{-12}$ S. This discrepancy in the values of conduction between the two models is consistent with the observation of increasing the permeation rates via the quantum tunneling effect, according to the THz trapped ion model. Furthermore, the quantum conductance values ranging

between $10^{-5}-10^{-12}$ S can be achieved by a kinetic energy $KE=1\times10^{-20}$ J, which is less than the energy barrier values ranging between $(1-2)\times10^{-20}$ J, as represented in Figure 7. This is consistent with the observation of the decrease in the kinetic energy requirement to cross the barrier according to the THz trapped ion model. Hence, this experimental model is a promising tool to validate the quantum tunneling of ions through the closed gate, and it will get more verification if THz resonance fluorescence and the intense field non-resonant effect, which have been proposed theoretically [54], are applied to detect the quantum tunneling. Additionally, a well-known experimental method called the kinetic isotope effect (KIE) has been used to verify the mass-dependent quantum tunneling at the rate of an enzymatic reaction [55–57]. This effect states that isotopes with different masses can yield different and significant rates that are mediated by quantum tunneling and cannot be observed if the process is mediated classically. Here, we will choose two stable potassium isotopes $K^{39}$ ($m_{K39}=6.5\times10^{-26}$ kg) and $K^{41}$ ($m_{K41}=6.8\times10^{-26}$ kg) to show that a minute difference in the mass can influence the quantum tunneling probability. See Figure 20. We did not choose sodium isotopes because sodium does not have stable isotopes.

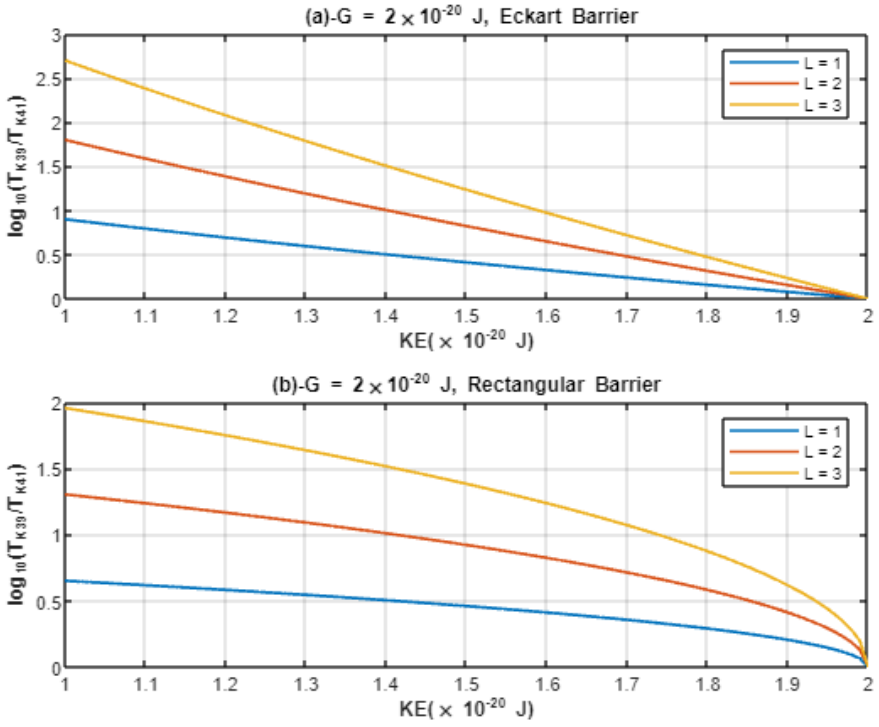


**Figure 20.** (a): The difference between the two stable potassium isotopes in terms of tunneling probability for the Eckart barrier. (b): The difference between the two stable potassium isotopes in terms of tunneling probability for the rectangular barrier.

Figure 20 shows the kinetic isotope effect of potassium ions, which becomes more obvious at lower values of kinetic energy and higher values of gate length. Also, changing the barrier's shape affects the degree of the difference between the two isotopes. For example, the Eckart barrier is associated with a larger difference between the two isotopes especially, at lower kinetic energy values. These observations can be used to validate the quantum tunneling model particularly, if the THz trapped ion model has been applied.

In addition, the most intriguing experimental observation made for the classical methods that can be related to our model is the paradoxical hyperexcitability caused by the gain-of-function (GOF) mutations [58,59]. Several explanations have been proposed to understand this unexpected effect, including the following.1) These GOF mutations occur in inhibitory neurons and thus disinhibition results in hyper-excitability [60]. 2) These mutations increase the rate of the repolarization phase for action potentials; thus, their frequency will increase and hyperexcitability is expected [61]. 3) These mutations trigger hyperpolarization-activated non-selective cationic current that depolarizes the membrane potential; thus, increases excitability [62]. Here, our model can provide another method, based on the quantum tunneling of potassium ions, that can depolarize the membrane potential directly without the event of hyperpolarization. Accordingly, if the THz trapped ion model is applied to potassium ions and proves the inward quantum tunneling of potassium ions, an electrophysiological study can be conducted to observe the membrane depolarization mediated by the quantum tunneling effect.

## 5. Summary

The present study showed that the quantum model exhibited several predictions that can contribute significantly to the pathogenesis of cardiac arrhythmias. The quantum model can achieve higher maximum single-channel conductance than the classical conductance of open channels. The quantum model requires the assumption that membrane depolarization can be induced by both sodium and potassium ions, while the classical model assumes that depolarization is induced only by sodium ions. Also, the degree of depolarization mediated by the quantum tunneling, especially if it is assisted by thermal energy, is expected to be higher when the barrier height decreases in response to pathological conditions. Furthermore, the quantum tunneling-induced depolarization is expected to be maintained for a longer duration because the quantum tunneling occurs through the different states of the closed gates, with different values of $G$, while the classical depolarization occurs only when the channels open. In addition, the thermal energy cost for the quantum depolarization is lower than that for the classical depolarization. Moreover, the success rate of reentry formation is higher for the quantum tunneling model due to the probabilistic nature of the quantum tunneling of ions. Finally, the quantum model predicts the formation of the anterograde and retrograde action potentials, without the requirement of the anatomical connections. See Table 1.

**Table 1.** Comparison between the quantum model and the classical model in terms of the mechanisms of cardiac arrhythmias.

| Criteria | The quantum model | The classical model |
|---|---|---|
| Maximum single-channel conductance | Higher | Lower |
| Depolarization by ions | Sodium and potassium | Only sodium |
| Degree of depolarization | High | Low |
| Maintenance of depolarization | High | Low |
| Thermal energy cost | Low | High |
| The likelihood of reentry formation | High | Low |
| Requirement of anatomical connection | No | Yes |

The overall pathogenesis of cardiac arrhythmias, from a quantum mechanical perspective, is

summarized in Figure 21.

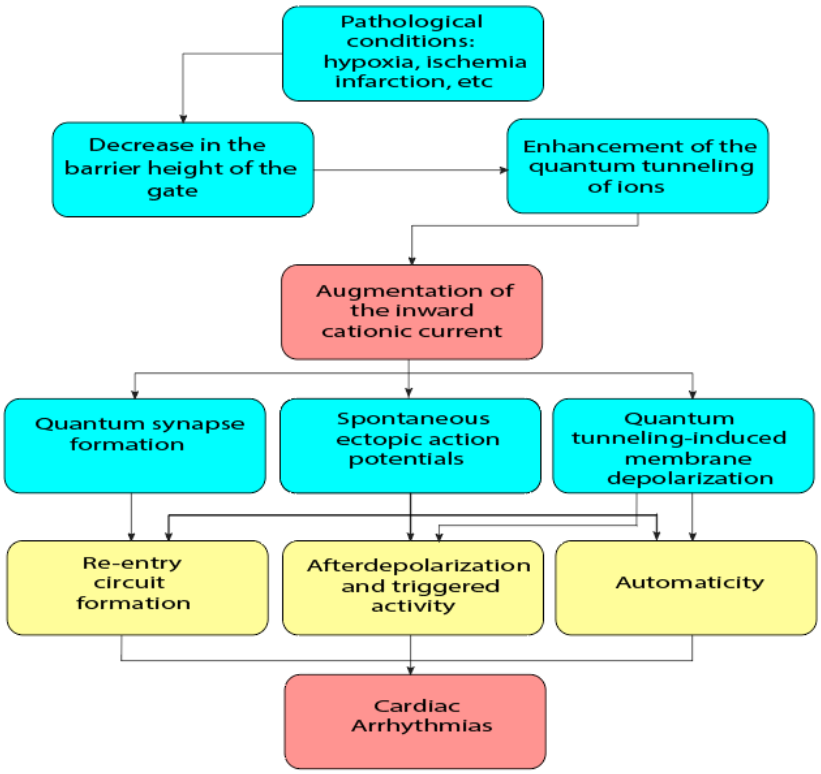


**Figure 21.** The figure represents a diagram that summarizes the pathogenesis of cardiac arrhythmias from a quantum mechanical perspective.

## Use of AI tools declaration

The authors declare that they have not used artificial antelligence tools in the creation of this article.

## Conflicts of interest

The authors declare no conflict of interest.

## Author contributions

Conceptualization, A.B.Q and M.I.A.I; methodology, A.B.Q; software, A.B.Q; validation, M.I.A.I. A.B.Q, M.B.A, A.H, A.A, M.H, D.I, M.N.A, I.M, K.A, E.J, M.A, M.B, M.A.M.A, A.D,N.A, A.A, I.M.I.I, L.A-H.; formal analysis, A.B.Q; investigation, M.I.A.I. A.B.Q, M.B.A, A.H, A.A, M.H, D.I, M.N.A, I.M, K.A, E.J, M.A, M.B, M.A.M.A, A.D,N.A, A.A, I.M.I.I, L.A-H.; resources, M.I.A.I. A.B.Q, M.B.A, A.H, A.A, M.H, D.I, M.N.A, I.M, K.A, E.J, M.A, M.B, M.A.M.A, A.D,N.A, A.A, I.M.I.I, L.A-H.; data curation, A.B.Q; writing—original draft preparation, A.B.Q; writing—review and editing, M.I.A.I. A.B.Q, M.B.A, A.H, A.A, M.H, D.I, M.N.A, I.M, K.A, E.J, M.A, M.B, M.A.M.A, A.D,N.A, A.A, I.M.I.I, L.A-H.; visualization, A.B.Q; supervision, L.A-H; project administration,

M.I.A.I and L.A-H.

**Funding:** This research received no external funding.

**Institutional review board statement:** Not applicable.

**Informed consent statement:** Not applicable.

**Data availability statement:** The data are available upon a reasonable request from the corresponding author.

## References

1. Huikuri HV, Castellanos A, Myerburg RJ (2001) Sudden death due to cardiac arrhythmias. *New Engl J Med* 345: 1473–1482. https://doi.org/10.1056/NEJMra000650
2. Srinivasan NT, Schilling RJ (2018) Sudden cardiac death and arrhythmias. *Arrhyth Electrophysi Rev* 7: 111. https://doi.org/10.15420/aer.2018:15:2
3. John RM, Tedrow UB, Koplan BA, et al. (2012) Ventricular arrhythmias and sudden cardiac death. *Lancet* 380: 1520–1529. https://doi.org/10.1016/S0140-6736(12)61413-5
4. Janse MJ, Wit AL (1989) Electrophysiological mechanisms of ventricular arrhythmias resulting from myocardial ischemia and infarction. *Physiol Rev* 69: 1049–1169. https://doi.org/10.1152/physrev.1989.69.4.1049
5. Peretto G, Sala S, Rizzo S, et al. (2019) Arrhythmias in myocarditis: state of the art. *Heart Rhythm* 16: 793–801. https://doi.org/10.1016/j.hrthm.2018.11.024
6. Kumar S, Stevenson WG, John RM (2015) Arrhythmias in dilated cardiomyopathy. *Card Electrophy Clin* 7: 221–233. https://doi.org/10.1016/j.hrthm.2018.11.024
7. Tisdale JE, Chung MK, Campbell KB, et al. (2020) Drug-induced arrhythmias: a scientific statement from the American Heart Association. *Circulation* 142: e214–233. https://doi.org/10.1161/CIR.0000000000000905
8. Behere SP, Weindling SN (2015) Inherited arrhythmias: The cardiac channelopathies. *Ann Pediat Cardiol* 8: 210. https://doi.org/10.4103/0974-2069.164695
9. FISCH C (1973) Relation of electrolyte disturbances to cardiac arrhythmias. *Circulation* 47: 408–419. https://doi.org/10.1161/01.CIR.47.2.408
10. Tse G (2016) Mechanisms of cardiac arrhythmias. *J Arrhythm* 32: 75–81. https://doi.org/10.1016/j.joa.2015.11.003
11. Antzelevitch C, Burashnikov A (2011) Overview of basic mechanisms of cardiac arrhythmia. *Card Electrophy Clin* 3: 23-45. https://doi.org/10.1016/j.ccep.2010.10.012
12. Marbán E (2002) Cardiac channelopathies. *Nature* 415: 213–218. https://doi.org/10.1038/415213a
13. Franz MR, Cima R, Wang D, et al. (1992) Electrophysiological effects of myocardial stretch and mechanical determinants of stretch-activated arrhythmias. *Circulation* 86: 968–978. https://doi.org/10.1161/01.CIR.86.3.968

14. Morand J, Arnaud C, Pepin JL, et al. (2018) Chronic intermittent hypoxia promotes myocardial ischemia-related ventricular arrhythmias and sudden cardiac death. *Sci Rep* 8: 1–8. https://doi.org/10.1038/s41598-018-21064-y
15. Orchard CH, Cingolani HE (1994) Acidosis and arrhythmias in cardiac muscle. *Card Res* 28: 1312–1319. https://doi.org/10.1093/cvr/28.9.1312
16. Morris CE (2011) Voltage-gated channel mechanosensitivity: fact or friction? *Front Physiol* 2: 25. https://doi.org/10.3389/fphys.2011.00025
17. Dehghani-Samani A, Madreseh-Ghahfarokhi S, Dehghani-Samani A (2019) Mutations of voltage-gated ionic channels and risk of severe cardiac arrhythmias. *Acta Cardiol Sin* 35: 99. https://doi.org/10.6515%2FACS.201903_35(2).20181028A
18. Li Q, Huang H, Liu G, et al. (2009) Gain-of-function mutation of Nav1. 5 in atrial fibrillation enhances cellular excitability and lowers the threshold for action potential firing. *Biochem Biophys Res Commun* 380: 132–137. https://doi.org/10.1016/j.bbrc.2009.01.052
19. Moskalenko A (2014) *Cardiac Arrhythmias Mechanisms, Pathophysiology, and Treatment*, 1–162. https://doi.org/10.5772/57008
20. Cardiac Arrhythmia Suppression Trial (CAST) Investigators (1989) Preliminary report: effect of encainide and flecainide on mortality in a randomized trial of arrhythmia suppression after myocardial infarction. *N Engl J Med* 321: 406–412. https://doi.org/10.1056/nejm198908103210629
21. Brooks MM, Gorkin L, Schron EB, et al. (1994) Moricizine and quality of life in the Cardiac Arrhythmia Suppression Trial II (CAST II). *Control Clin Trials* 15: 437–449. https://doi.org/10.1016/0197-2456(94)90002-7
22. Kurian TK, Efimov IR (2010) Mechanisms of fibrillation: Neurogenic or myogenic? reentrant or focal? multiple or single?: Still puzzling after 160 years of inquiry. *J Card Electrophysiol* 21: 1274. https://doi.org/10.1111%2Fj.1540-8167.2010.01820.x
23. Calvillo L, Redaelli V, Ludwig N, et al. (2022) Quantum biology research meets pathophysiology and therapeutic mechanisms: a biomedical perspective. *Quantum Rep* 4: 148–172. https://www.mdpi.com/2624-960X/4/2/11
24. Kim Y, Bertagna F, D'souza EM, et al. (2021) Quantum biology: An update and perspective. *Quantum Rep* 3: 80–126. https://www.mdpi.com/2624-960X/3/1/6
25. Cao J, Cogdell RJ, Coker DF, et al. (2020) Quantum biology revisited. *Sci Adv* 6: eaaz4888. https://doi.org/10.1126/sciadv.aaz4888
26. Slocombe L, Sacchi M, Al-Khalili (2022) An open quantum systems approach to proton tunnelling in DNA. *Commun Phys* 5: 109. https://doi.org/10.1038/s42005-022-00881-8
27. Sutcliffe MJ, Scrutton NS (2002) A new conceptual framework for enzyme catalysis: Hydrogen tunneling coupled to enzyme dynamics in flavoprotein and quinoprotein enzymes. *Eur J Biochem* 269: 3096–3102. https://doi.org/10.1046/j.1432-1033.2002.03020.x
28. Qaswal AB (2019) Quantum tunneling of ions through the closed voltage-gated channels of the biological membrane: A mathematical model and implications. *Quantum Rep* 1: 219–225. https://www.mdpi.com/2624-960X/1/2/19
29. Miller DA (2008) Quantum mechanics for scientists and engineers. Cambridge University Press.
30. Aryal P, Sansom MS, Tucker SJ (2015) Hydrophobic gating in ion channels. *J Mol Biol* 427: 121–130. https://doi.org/10.1016/j.jmb.2014.07.030

31. Oelstrom K, Goldschen-Ohm MP, Holmgren M, et al. (2014) Evolutionarily conserved intracellular gate of voltage-dependent sodium channels. *Nat Commun* 5: 3420. https://doi.org/10.1038/ncomms4420
32. Jensen MØ, Borhani DW, Lindorff-Larsen K, et al. (2010) Principles of conduction and hydrophobic gating in K+ channels. *Proceedings of the National Academy of Sciences* 107: 5833–5838. https://doi.org/10.1073/pnas.0911691107
33. Trick JL, Aryal P, Tucker SJ, et al. (2015) Molecular simulation studies of hydrophobic gating in nanopores and ion channels. *Biochem Society Transact* 43: 146–150. https://doi.org/10.1042/BST20140256
34. Rao S, Klesse G, Lynch CI, et al. (2021) Molecular simulations of hydrophobic gating of pentameric ligand gated ion channels: insights into water and ions. *J Phys Chem B* 125: 981–994. https://doi.org/10.1021/acs.jpcb.0c09285
35. Chandra AK (1974) *Introductory Quantum Chemistry*, 4 Ed., McGraw-Hill.
36. Miyazaki T (2004) *Atom Tunneling Phenomena in Physics, Chemistry and Biology*, Berlin: Springer Science & Business Media.
37. Serway RA, Moses CJ, Moyer CA (2004) Modern physics.
38. Eckart C (1930) The penetration of a potential barrier by electrons. *Phys Rev* 35: 1303. https://doi.org/10.1103/PhysRev.35.1303
39. Zhu F, Hummer G (2012) Drying transition in the hydrophobic gate of the GLIC channel blocks ion conduction. *Biophys J* 103: 219–227. http://dx.doi.org/10.1016/j.bpj.2012.06.003
40. Rao S, Lynch CI, Klesse G, et al. (2018) Water and hydrophobic gates in ion channels and nanopores. *Faraday Discuss* 209: 231–247. https://doi.org/10.1039/C8FD00013A
41. Neale C, Chakrabarti N, Pomorski P, et al. (2015) Hydrophobic gating of ion permeation in magnesium channel CorA. *PLoS Comput Biol* 11: e1004303. https://doi.org/10.1371/journal.pcbi.1004303
42. Khavrutskii IV, Gorfe AA, Lu B, et al. (2009) Free energy for the permeation of $Na^+$ and $Cl^-$ ions and their ion-pair through a zwitterionic dimyristoyl phosphatidylcholine lipid bilayer by umbrella integration with harmonic fourier beads. *J Am Chem Society* 131: 1706–1716. https://doi.org/10.1021/ja8081704
43. Vorobyov I, Olson TE, Kim JH, et al. (2014) Ion-induced defect permeation of lipid membranes. *Biophys J* 106: 586–597. http://dx.doi.org/10.1016/j.bpj.2013.12.027
44. Leontiadou H, Mark AE, Marrink SJ (2007) Ion transport across transmembrane pores. *Biophys J* 92: 4209–4215. http://dx.doi.org/10.1529/biophysj.106.101295
45. Zhang HY, Xu Q, Wang YK, et al. (2016) Passive transmembrane permeation mechanisms of monovalent ions explored by molecular dynamics simulations. *J Chem Theory Comput* 12: 4959–4969. https://doi.org/10.1021/acs.jctc.6b00695
46. Chen F, Hihath J, Huang Z, et al. (2007) Measurement of single-molecule conductance. *Annu Rev Phys Chem* 58: 535–564. https://doi.org/10.1146/annurev.physchem.58.032806.104523
47. Qaswal AB (2020) Quantum electrochemical equilibrium: Quantum version of the Goldman–Hodgkin–Katz equation. *Quantum Rep* 2: 266–277. https://www.mdpi.com/2624-960X/2/2/17
48. Qaswal AB (2021) The role of quantum tunneling of ions in the pathogenesis of the cardiac arrhythmias due to channelopathies, ischemia, and mechanical stretch. *Biophysics* 66: 637–641. https://doi.org/10.1134/S0006350921040072

49. Ababneh O, Qaswal AB, Alelaumi A, et al. (2021) Proton quantum tunneling: Influence and relevance to acidosis-induced cardiac arrhythmias/cardiac arrest. *Pathophysiology* 28: 400–436. https://www.mdpi.com/1873-149X/28/3/27
50. Zhang XC, Yang H, Liu Z, et al. (2018) Thermodynamics of voltage-gated ion channels. *Biophys Rep* 4: 300–319. https://doi.org/10.1016/j.celrep.2021.109931
51. Summhammer J, Salari V, Bernroider G (2012) A quantum-mechanical description of ion motion within the confining potentials of voltage-gated ion channels. *J Integr Neurosci* 11: 123–135. https://doi.org/10.1142/S0219635212500094
52. Summhammer J, Sulyok G, Bernroider G (2018) Quantum dynamics and non-local effects behind ion transition states during permeation in membrane channel proteins. *Entropy* 20: 558. https://doi.org/10.1142/S0219635212500094
53. Summhammer J, Sulyok G, Bernroider G (2020) Quantum mechanical coherence of $K^+$ ion wave packets increases conduction in the KcsA ion channel. *Appl Sci.* 10: 4250. https://www.mdpi.com/2076-3417/10/12/4250
54. Wang K, Wang S, Yang L, et al. (2021) THz trapped ion model and THz spectroscopy detection of potassium channels. *Nano Res* 15: 3825–3833. https://doi.org/10.1007/s12274-021-3965-z
55. Karandashev K, Xu ZH, Meuwly M, et al. (2017) Kinetic isotope effects and how to describe them. *Struct Dynam* 4: 061501. https://doi.org/10.1063/1.4996339
56. Sen A, Kohen A (2010) Enzymatic tunneling and kinetic isotope effects: chemistry at the crossroads. *J Phys Org Chem* 23: 613–619. https://doi.org/10.1002/poc.1633
57. Eckhardt AK, Gerbig D, Schreiner PR (2018) Heavy atom secondary kinetic isotope effect on H-tunneling. *J Phys Chem A* 122: 1488–1495. https://doi.org/10.1021/acs.jpca.7b12118
58. Nappi P, Miceli F, Soldovieri MV, et al. (2020) Epileptic channelopathies caused by neuronal Kv7 (KCNQ) channel dysfunction. *Pflüg Arch-Eur J Phy* 472: 881–898. https://doi.org/10.1007/s00424-020-02404-2
59. Niday Z, Tzingounis AV (2018) Potassium channel gain of function in epilepsy: an unresolved paradox. *Neurosci* 24: 368–380. https://doi.org/10.1177/1073858418763752
60. Miceli F, Soldovieri MV, Ambrosino P, et al. (2015) Early-onset epileptic encephalopathy caused by gain-of-function mutations in the voltage sensor of Kv7. 2 and Kv7. 3 potassium channel subunits. *J Neurosci* 35: 3782–3793. https://doi.org/10.1523/JNEUROSCI.4423-14.2015
61. Du W, Bautista JF, Yang H, et al. (2005) Calcium-sensitive potassium channelopathy in human epilepsy and paroxysmal movement disorder. *Nat Genet* 37: 733–738. https://doi.org/10.1038/ng1585
62. Robinson RB, Siegelbaum SA (2003) Hyperpolarization-activated cation currents: from molecules to physiological function. *Annu Rev Physiol* 65: 453–480. https://doi.org/10.1146/annurev.physiol.65.092101.142734



AIMS Press